Solvable Markov random field model in color image restoration

Kazuyuki Tanaka* and Tsuyoshi Horiguchi†
Department of Computer and Mathematical Sciences, Graduate School of Information Science, Tohoku University, Aramaki-aza-aoba 04, Aoba-ku, Sendai 980-8579, Japan

(Received 10 July 2001; revised manuscript received 18 December 2001; published 11 April 2002)

We propose a scheme for image restoration of full color images by means of a solvable probabilistic model in the red-green-blue space. A special case of our solvable probabilistic model is equivalent to a multicomponent Gaussian model in the statistical mechanics. Exact closed expressions of the evidence and the expectation value of intensity at each pixel in our solvable probabilistic model can be obtained by using multidimensional Gaussian integral formulas and a discrete Fourier transform. In the present paper, the degradation process is assumed to be an additive white Gaussian noise. Hyperparameters are determined so as to maximize the evidence that is expressed in terms of the partition function in our solvable probabilistic model. This work is a pioneering work for the Bayesian approach to the color image restoration by means of the statistical-mechanical technique.

DOI: 10.1103/PhysRevE.65.046142 PACS number(s): 02.50.−r, 05.20.−y

I. INTRODUCTION

Probabilistic image processing is a very powerful approach and hence not only computer and mathematical scientists but also statistical physicists are interested in such an approach [1]. In the probabilistic image processing, a probabilistic model is constructed by means of Bayes statistics and usually has a Gibbs distribution. It was suggested that the probabilistic image processing has a very close relationship to the spin glass theory in statistical mechanics [1]. Geman and co-workers [2,3] proposed a formulation for image restoration by means of Bayes statistics and the simulated annealing. Their model is based on a Markov random field, in which the state of a pixel depends only on the states of its nearest neighbor pixels [2]. Many investigations by the Bayesian approaches in terms of the Markov random fields were done to more practical applications in the image processing [4,5].

Color image processing is one of fundamental and interesting problems in image and vision computing. Angelopoulos and Pitas [6] dealt with a design of multichannel Wiener filter, which is a familiar technique in the image processing for color image restoration based on a multichannel autoregressive model. Panjwani and Healey [7] proposed an unsupervised segmentation algorithm for color textures by using a Markov random field (MRF) model with interactions between different color planes in the RGB space. Here the notations R, G and B mean red, green, and blue, respectively. Recently, some algorithms for color image segmentation based on the maximum *a posteriori* estimation in MRF models were also proposed in an $L^*u^*v^*$ space, which is related to the RGB values by nonlinear transformations [8,9]. The components u^* and v^* carry the chromatic information and the other component L^* can be regarded as the information for brightness [10]. However, a color image restoration algorithm by using MRF models has not been proposed yet in any color space.

Some statistical physicists were also interested in the Bayesian information processing by means of a solvable probabilistic model. Vicente *et al.* [11] studied a belief propagation algorithm for error-correcting codes by means of a solvable Ising model on a cactus tree. Nishimori and Wong [12] studied a performance of Bayesian image processing by means of an infinite range Ising model with random external fields and uniform interactions. They suggested that the highest performance of Bayesian image processing is given on the Nishimori line for each probabilistic model from an exact inequality and some detailed calculations by using the replica method. Nishimori [13] showed also that the Gaussian model is applicable to image restoration in gray-level monochrome images and that image restoration framework by means of maximum *a posteriori* estimation in the Gaussian model is equivalent to the Wiener filter. Molina [14] presented some iterative algorithms for a hyperparameter estimation of a probabilistic model, in which the *a priori* probability is assumed to be a conditional autoregressive (CAR) model or a simultaneous autoregressive (SAR) model, in the aid of a saddle point approximation. The CAR model is equivalent to the Gaussian model in the statistical mechanics. Tanaka and Inoue [15] suggested that the expressions of some statistical quantities in both CAR and SAR models can be exactly given by using the multidimensional Gaussian integral formulas and the discrete Fourier transform. They extended such a solvable probabilistic model to more general solvable probabilistic models and gave an exact closed expression of evidence to estimate some hyperparameters only from a given degraded image.

In this paper, we propose a scheme for the image restoration of full color images by means of a solvable probabilistic model in the RGB space by extending the solvable probabilistic model for the monochrome image restoration given by Tanaka and Inoue [15]. In order to discuss about the most fundamental problem in color image restorations and clarify

*Electronic address: kazu@statp.is.tohoku.ac.jp; FAX: +81-22-217-5851.
†Electronic address: tsuyoshi@statp.is.tohoku.ac.jp

 ©2002 The American Physical Society

their nature, we restrict our degradation process to an additive white Gaussian noise, which is one of the most popular degradation models in image processing. In Sec. II, we construct a solvable probabilistic model for the image restoration of color images and derive an exact expression of evidence to estimate hyperparameters and that of the expectation value of intensity of each component in a color at each pixel. In Sec. III, a practical algorithm and some numerical experiments are given. Concluding remarks are given in Sec. IV.

II. SOLVABLE PROBABILISTIC MODEL FOR COLOR IMAGE RESTORATION

We consider a color image on a square lattice $\mathbf{L}=\{(x,y)|\, x=0,1,\ldots,L_x-1,\, y=0,1,\ldots,L_y-1\}$. The lattice is assumed to consist of $|\mathbf{L}|$ pixels and to satisfy the periodic boundary conditions, so that the lattice is on a torus. Three components corresponding to three colors, namely, red, green, and blue, in a digital color image are assigned to each pixel. The colors on a pixel (x,y) in an original image and in a degraded image are denoted by

$$\vec{f}_{x,y}\equiv\begin{pmatrix} f_{x,y,\mathrm{red}} \\ f_{x,y,\mathrm{green}} \\ f_{x,y,\mathrm{blue}} \end{pmatrix} \quad \text{and} \quad \vec{g}_{x,y}\equiv\begin{pmatrix} g_{x,y,\mathrm{red}} \\ g_{x,y,\mathrm{green}} \\ g_{x,y,\mathrm{blue}} \end{pmatrix},$$

respectively. Now, we introduce the notation $\mathbf{K}$ defined by $\mathbf{K}\equiv\{\mathrm{red},\mathrm{green},\mathrm{blue}\}$. The configurations of the original image and of the given degraded image are represented by $\boldsymbol{f}=\{f_{x,y,\kappa}|(x,y)\in\mathbf{L},\ \kappa\in\mathbf{K}\}$ and $\boldsymbol{g}=\{g_{x,y,\kappa}|(x,y)\in\mathbf{L},\ \kappa\in\mathbf{K}\}$, respectively. Each variable $f_{x,y,\kappa}$ and $g_{x,y,\kappa}$ take any real number in the interval $(-\infty,+\infty)$. In recovering the original image $\boldsymbol{f}$ from the given degraded image $\boldsymbol{g}$, we use some *a priori* properties of the original image $\boldsymbol{f}$. We express sets of random variables representing the original and the degraded image by $\boldsymbol{F}=\{F_{x,y,\kappa}|(x,y)\in\mathbf{L},\ \kappa\in\mathbf{K}\}$ and $\boldsymbol{G}=\{G_{x,y,\kappa}|(x,y)\in\mathbf{L},\ \kappa\in\mathbf{K}\}$, respectively.

We adopt an additive white Gaussian noise $\mathcal{N}[0,\sigma^2]$ so that the conditional probability density function $\Pr\{\boldsymbol{G}=\boldsymbol{g}|\boldsymbol{F}=\boldsymbol{f},\sigma\}$ is assumed to be

$$\Pr\{\boldsymbol{G}=\boldsymbol{g}|\boldsymbol{F}=\boldsymbol{f},\sigma\}\equiv\frac{1}{Z_{\mathrm{noise}}(\sigma)}\exp\left(-\frac{1}{2\sigma^2}||\boldsymbol{g}-\boldsymbol{f}||^2\right), \tag{2.1}$$

where

$$Z_{\mathrm{noise}}(\sigma)\equiv(2\pi\sigma^2)^{3|\mathbf{L}|/2}, \tag{2.2}$$

$$||\boldsymbol{g}-\boldsymbol{f}||^2\equiv\sum_{(x,y)\in\mathbf{L}}\sum_{\kappa\in\mathbf{K}}(g_{x,y,\kappa}-f_{x,y,\kappa})^2. \tag{2.3}$$

Hence $||\cdot||^2$ is the square norm.

The *a priori* probability density function for the original image $\boldsymbol{f}$ is assumed to be

$$\Pr\{\boldsymbol{F}=\boldsymbol{f}|\boldsymbol{\alpha},\nu\}\equiv\frac{1}{Z_{\mathrm{prior}}(\boldsymbol{\alpha},\nu)}\times\exp\left(-\frac{1}{2}\sum_{\kappa\in\mathbf{K}}\sum_{\kappa'\in\mathbf{K}}\alpha'_{\kappa,\kappa'}\boldsymbol{f}^T\boldsymbol{C}(\kappa,\kappa')^{\nu}\boldsymbol{f}\right), \tag{2.4}$$

where

$$Z_{\mathrm{prior}}(\boldsymbol{\alpha},\nu)\equiv\int\exp\left(-\frac{1}{2}\sum_{\kappa\in\mathbf{K}}\sum_{\kappa'\in\mathbf{K}}\alpha_{\kappa,\kappa'}\boldsymbol{z}^T\boldsymbol{C}(\kappa,\kappa')^{\nu}\boldsymbol{z}\right)d\boldsymbol{z}. \tag{2.5}$$

Here $\boldsymbol{f}^T$ is the transpose of vector $\boldsymbol{f}$, and $\alpha_{\kappa,\kappa'}$ and ν are hyperparameters. The integral is defined by

$$\int d\boldsymbol{z}\equiv\int_{-\infty}^{+\infty}\int_{-\infty}^{+\infty}\cdots\int_{-\infty}^{+\infty}\times\prod_{(x,y)\in\mathbf{L}}dz_{x,y,\mathrm{red}}dz_{x,y,\mathrm{green}}dz_{x,y,\mathrm{blue}}. \tag{2.6}$$

$\boldsymbol{C}(\kappa,\kappa')$ $(\kappa,\kappa'\in\mathbf{K})$ is a $3|\mathbf{L}|\times3|\mathbf{L}|$ matrix whose $(x,y,\mu|x',y',\mu')$ element is defined by

$$\begin{aligned}\langle x,y,\mu|\boldsymbol{C}(\kappa,\kappa')|x',y',\mu'\rangle &\equiv\delta_{\kappa,\mu}\delta_{\kappa',\mu'}\times\left(\delta_{x,x'}\delta_{y,y'}-\frac{1}{4}\delta_{x,x'+1}\delta_{y,y'}\right.\\ &\left.-\frac{1}{4}\delta_{x,x'-1}\delta_{y,y'}-\frac{1}{4}\delta_{x,x'}\delta_{y,y'+1}-\frac{1}{4}\delta_{x,x'}\delta_{y,y'-1}\right)\end{aligned}$$

$$[(x,y),(x',y')\in\mathbf{L},\ \mu,\mu'\in\mathbf{K}]. \tag{2.7}$$

Here $\delta_{x,y}$ is Kronecker's delta. In the case of $\nu=2$, the *a priori* probability density function is equivalent to the one of the multichannel SAR model characterized by

$$\vec{f}_{x,y}-\frac{1}{4}(\vec{f}_{x+1,y}+\vec{f}_{x-1,y}+\vec{f}_{x,y+1}+\vec{f}_{x,y-1})\sim\mathcal{N}[\vec{0},\boldsymbol{\alpha}^{-1}]. \tag{2.8}$$

Here, $\vec{0}$ is the three-dimensional zero vector and $\mathcal{N}[\vec{0},\boldsymbol{\alpha}^{-1}]$ is a three-dimensional Gaussian distribution whose average of each component is zero and covariant matrix is $\boldsymbol{\alpha}^{-1}$. The energy function of the multichannel SAR model is rewritten as follows:

$$\frac{1}{2}\sum_{\kappa\in\mathbf{K}}\sum_{\kappa'\in\mathbf{K}}\alpha_{\kappa,\kappa'}\boldsymbol{f}^T\boldsymbol{C}(\kappa,\kappa')^2\boldsymbol{f}$$
$$=\sum_{(x,y)\in\mathbf{L}}\sum_{\kappa\in\mathbf{K}}\sum_{\kappa'\in\mathbf{K}}\alpha_{\kappa,\kappa'}\left(f_{x,y,\kappa}-\frac{1}{4}(f_{x+1,y,\kappa}+f_{x-1,y,\kappa}+f_{x,y+1,\kappa}+f_{x,y-1,\kappa})\right)\left(f_{x,y,\kappa'}-\frac{1}{4}(f_{x+1,y,\kappa'}+f_{x-1,y,\kappa'}+f_{x,y+1,\kappa'}+f_{x,y-1,\kappa'})\right). \tag{2.9}$$

In the case of $\nu=1$, the *a priori* probability density function is equivalent to the one of the multichannel CAR model as follows:

$$\vec{f}_{x,y}-\vec{f}_{x+1,y}\sim\mathcal{N}[\vec{0},\boldsymbol{\alpha}^{-1}],\quad \vec{f}_{x,y}-\vec{f}_{x,y+1}\sim\mathcal{N}[\vec{0},\boldsymbol{\alpha}^{-1}]. \tag{2.10}$$

The energy function of the multi-channel CAR model is rewritten as follows:

$$\frac{1}{2}\sum_{\kappa\in\mathbf{K}}\sum_{\kappa'\in\mathbf{K}}\alpha_{\kappa,\kappa'}\boldsymbol{f}^T\boldsymbol{C}(\kappa,\kappa')\boldsymbol{f}$$
$$=\sum_{(x,y)\in\mathbf{L}}\sum_{\kappa\in\mathbf{K}}\sum_{\kappa'\in\mathbf{K}}\alpha_{\kappa,\kappa'}[(f_{x,y,\kappa}-f_{x+1,y,\kappa})\times(f_{x,y,\kappa'}-f_{x+1,y,\kappa'})+(f_{x,y,\kappa}-f_{x,y+1,\kappa})\times(f_{x,y,\kappa'}-f_{x,y+1,\kappa'})]. \tag{2.11}$$

Equations (2.10) and (2.8) mean that the coefficients $\alpha_{\kappa,\kappa'}$ $(\kappa\neq\kappa')$ express the correlation between the different color planes in the *RGB* picture information. We remark that both SAR and CAR models for the monochrome image restoration have been proposed by Molina [14].

In the Bayes formula, the *a posteriori* probability density function $\Pr\{\boldsymbol{F}=\boldsymbol{f}|\boldsymbol{G}=\boldsymbol{g},\boldsymbol{\alpha},\nu,\sigma\}$, that the original image is $\boldsymbol{f}$ when the given degraded image is $\boldsymbol{g}$, is expressed as

$$\Pr\{\boldsymbol{F}=\boldsymbol{f}|\boldsymbol{G}=\boldsymbol{g},\boldsymbol{\alpha},\nu,\sigma\}=\frac{\Pr\{\boldsymbol{G}=\boldsymbol{g}|\boldsymbol{F}=\boldsymbol{f},\sigma\}\Pr\{\boldsymbol{F}=\boldsymbol{f}|\boldsymbol{\alpha},\nu\}}{\int\Pr\{\boldsymbol{G}=\boldsymbol{g}|\boldsymbol{F}=\boldsymbol{z},\sigma\}\Pr\{\boldsymbol{F}=\boldsymbol{z}|\boldsymbol{\alpha},\nu\}d\boldsymbol{z}}. \tag{2.12}$$

An estimate of hyperparameters $\boldsymbol{\alpha}$, ν, and σ is determined so as to maximize the evidence $\Pr\{\boldsymbol{G}=\boldsymbol{g}|\boldsymbol{\alpha},\nu,\sigma\}$ [16–18]:

$$\Pr\{\boldsymbol{G}=\boldsymbol{g}|\boldsymbol{\alpha},\nu,\sigma\}\equiv\int\Pr\{\boldsymbol{G}=\boldsymbol{g}|\boldsymbol{F}=\boldsymbol{z},\sigma\}\Pr\{\boldsymbol{F}=\boldsymbol{z}|\boldsymbol{\alpha},\nu\}d\boldsymbol{z}. \tag{2.13}$$

The maximizers of evidence $\Pr\{\boldsymbol{G}=\boldsymbol{g}|\boldsymbol{\alpha},\nu,\sigma\}$ are denoted by $\hat{\boldsymbol{\alpha}}$, $\hat{\nu}$, and $\hat{\sigma}$, such that

$$(\hat{\boldsymbol{\alpha}},\hat{\nu},\hat{\sigma})=\arg\max_{(\boldsymbol{\alpha},\nu,\sigma)}\Pr\{\boldsymbol{G}=\boldsymbol{g}|\boldsymbol{\alpha},\nu,\sigma\}. \tag{2.14}$$

For the obtained estimates $\hat{\boldsymbol{\alpha}}$, $\hat{\nu}$, and $\hat{\sigma}$, the restored image $\hat{\boldsymbol{f}}\equiv\{\hat{f}_{x,y,\kappa}|(x,y)\in\mathbf{L},\ \kappa\in\mathbf{K}\}$ is determined by

$$\hat{f}_{x,y,\kappa}\equiv\int z_{x,y,\kappa}\Pr\{\boldsymbol{F}=\boldsymbol{z}|\boldsymbol{G}=\boldsymbol{g},\hat{\boldsymbol{\alpha}},\hat{\nu},\hat{\sigma}\}d\boldsymbol{z}$$
$$[(x,y)\in\mathbf{L},\ \ \kappa\in\mathbf{K}]. \tag{2.15}$$

By introducing the unitary matrix $\boldsymbol{U}$ defined by

$$\langle x,y,\kappa|\boldsymbol{U}|p,q,\kappa'\rangle\equiv\frac{1}{\sqrt{|\mathbf{L}|}}\exp\left(-i\frac{2\pi px}{L_x}-i\frac{2\pi qy}{L_y}\right), \tag{2.16}$$

the matrix $\boldsymbol{C}(\kappa,\kappa')$ can be diagonalized as follows:

$$\langle p,q,\mu|\boldsymbol{U}^{-1}\boldsymbol{C}(\kappa,\kappa')\boldsymbol{U}|p',q',\mu'\rangle=\delta_{\kappa,\mu}\delta_{\kappa',\mu'}\delta_{p,p'}\delta_{q,q'}\lambda(p,q)$$
$$[(p,q),(p',q')\in\mathbf{L},\mu,\mu'\in\mathbf{K}], \tag{2.17}$$

where

$$\lambda(p,q)\equiv1-\frac{1}{2}\cos\left(\frac{2\pi p}{L_x}\right)-\frac{1}{2}\cos\left(\frac{2\pi q}{L_y}\right), \tag{2.18}$$

and $Z_{\text{prior}}(\boldsymbol{\alpha},\nu)$ can be expressed in the following form:

$$Z_{\text{prior}}(\boldsymbol{\alpha},\nu)=(2\pi)^{3|\mathbf{L}|/2}\left\{\det\left(\sum_{\kappa\in\mathbf{K}}\sum_{\kappa'\in\mathbf{K}}\alpha_{\kappa,\kappa'}\boldsymbol{C}(\kappa,\kappa')^{\nu}\right)\right\}^{-1/2}$$
$$=(2\pi)^{3|\mathbf{L}|/2}\prod_{(p,q)\in\mathbf{L}}\{\lambda(p,q)^{3\nu}\det(\boldsymbol{\alpha})\}^{-1/2}, \tag{2.19}$$

where

$$\boldsymbol{\alpha}\equiv\begin{pmatrix}\alpha_{\text{red,red}} & \alpha_{\text{red,green}} & \alpha_{\text{red,blue}}\\ \alpha_{\text{green,red}} & \alpha_{\text{green,green}} & \alpha_{\text{green,blue}}\\ \alpha_{\text{blue,red}} & \alpha_{\text{blue,green}} & \alpha_{\text{blue,blue}}\end{pmatrix}. \tag{2.20}$$

By substituting Eqs. (2.1) and (2.4) to Eq. (2.12), the *a posteriori* probability density function is obtained as follows:

$$\Pr\{\boldsymbol{F}=\boldsymbol{f}|\boldsymbol{G}=\boldsymbol{g},\boldsymbol{\alpha},\nu,\sigma\}=\frac{1}{Z_{\text{posterior}}(\boldsymbol{\alpha},\nu,\sigma)}\exp[-H(\boldsymbol{f}|\boldsymbol{g},\boldsymbol{\alpha},\nu,\sigma)], \tag{2.21}$$

where

$$Z_{\text{posterior}}(\boldsymbol{\alpha},\nu,\sigma)\equiv\int \exp[-H(\boldsymbol{z}|\boldsymbol{g},\boldsymbol{\alpha},\nu,\sigma)]d\boldsymbol{z}, \tag{2.22}$$

and

$$\begin{aligned}H(\boldsymbol{f}|\boldsymbol{g},\boldsymbol{\alpha},\nu,\sigma)&\equiv\frac{1}{2\sigma^2}||\boldsymbol{f}-\boldsymbol{g}||^2+\frac{1}{2}\boldsymbol{f}^T\left(\sum_{\kappa\in\mathbf{K}}\sum_{\kappa'\in\mathbf{K}}\alpha_{\kappa,\kappa'}\boldsymbol{C}(\kappa,\kappa')^\nu\right)\boldsymbol{f}\\&=\frac{1}{2\sigma^2}\left[-\boldsymbol{f}\left(\boldsymbol{I}+\sigma^2\sum_{\kappa\in\mathbf{K}}\sum_{\kappa'\in\mathbf{K}}\alpha_{\kappa,\kappa'}\boldsymbol{C}(\kappa,\kappa')^\nu\right)^{-1}\boldsymbol{g}\right]^T\left(\boldsymbol{I}+\sigma^2\sum_{\kappa\in\mathbf{K}}\sum_{\kappa'\in\mathbf{K}}\alpha_{\kappa,\kappa'}\boldsymbol{C}(\kappa,\kappa')^\nu\right)\\&\quad\times\left[\boldsymbol{f}-\left(\boldsymbol{I}+\sigma^2\sum_{\kappa\in\mathbf{K}}\sum_{\kappa'\in\mathbf{K}}\alpha_{\kappa,\kappa'}\boldsymbol{C}(\kappa,\kappa')^\nu\right)^{-1}\boldsymbol{g}\right]\\&\quad+\frac{1}{2}\boldsymbol{g}^T\left(\sum_{\kappa\in\mathbf{K}}\sum_{\kappa'\in\mathbf{K}}\alpha_{\kappa,\kappa'}\boldsymbol{C}(\kappa,\kappa')^\nu\right)\left(\boldsymbol{I}+\sigma^2\sum_{\kappa\in\mathbf{K}}\sum_{\kappa'\in\mathbf{K}}\alpha_{\kappa,\kappa'}\boldsymbol{C}(\kappa,\kappa')^\nu\right)^{-1}\boldsymbol{g}.\end{aligned} \tag{2.23}$$

The partition function $Z_{\text{posterior}}(\boldsymbol{\alpha},\nu,\sigma)$ is expressed in the following form:

$$\begin{aligned}Z_{\text{posterior}}(\boldsymbol{\alpha},\nu,\sigma)&=(2\pi\sigma^2)^{3|\mathbf{L}|/2}\left\{\det\left(\boldsymbol{I}+\sigma^2\sum_{\kappa\in\mathbf{K}}\sum_{\kappa'\in\mathbf{K}}\alpha_{\kappa,\kappa'}\boldsymbol{C}(\kappa,\kappa')^\nu\right)\right\}^{-1/2}\\&\quad\times\exp\left\{-\frac{1}{2}\boldsymbol{g}^T\left(\sum_{\kappa\in\mathbf{K}}\sum_{\kappa'\in\mathbf{K}}\alpha_{\kappa,\kappa'}\boldsymbol{C}(\kappa,\kappa')^\nu\right)\left(\boldsymbol{I}+\sigma^2\sum_{\kappa\in\mathbf{K}}\sum_{\kappa'\in\mathbf{K}}\alpha_{\kappa,\kappa'}\boldsymbol{C}(\kappa,\kappa')^\nu\right)^{-1}\boldsymbol{g}\right\}\\&=(2\pi\sigma^2)^{3|\mathbf{L}|/2}\prod_{(p,q)\in\mathbf{L}}\{\det[\boldsymbol{e}+\lambda(p,q)^\nu\boldsymbol{\alpha}]\}^{-1/2}\\&\quad\times\exp\left\{-\frac{1}{2}\sum_{(p,q)\in\mathbf{L}}\{\vec{G}^\dagger(p,q)\lambda(p,q)^\nu\boldsymbol{\alpha}[\boldsymbol{e}+\sigma\lambda(p,q)^\nu\boldsymbol{\alpha}]^{-1}\vec{G}(p,q)\}\right\},\end{aligned} \tag{2.24}$$

where

$$\vec{G}(p,q)=\begin{pmatrix}G_{\text{red}}(p,q)\\G_{\text{green}}(p,q)\\G_{\text{blue}}(p,q)\end{pmatrix}\equiv\frac{1}{\sqrt{|\mathbf{L}|}}\sum_{(x,y)\in\mathbf{L}}\begin{pmatrix}g_{x,y,\text{red}}\\g_{x,y,\text{green}}\\g_{x,y,\text{blue}}\end{pmatrix}\exp\left(-i\frac{2\pi px}{L_x}-i\frac{2\pi qy}{L_y}\right), \tag{2.25}$$

$$\vec{G}^\dagger(p,q)\equiv\frac{1}{\sqrt{|\mathbf{L}|}}\sum_{(x,y)\in\mathbf{L}}(g_{x,y,\text{red}},g_{x,y,\text{green}},g_{x,y,\text{blue}})\exp\left(i\frac{2\pi px}{L_x}+i\frac{2\pi qy}{L_y}\right), \tag{2.26}$$

and $\boldsymbol{e}$ is a 3×3 unit matrix. By using Eqs. (2.2), (2.19), and (2.24), the logarithm of evidence can be expressed in the following form:

$$\ln(\Pr\{\boldsymbol{G}=\boldsymbol{g}|\boldsymbol{\alpha},\nu,\sigma\})=\ln\left(\frac{Z_{\text{posterior}}(\boldsymbol{\alpha},\nu,\sigma)}{Z_{\text{noise}}(\sigma)Z_{\text{prior}}(\boldsymbol{\alpha},\nu)}\right)$$
$$=-\frac{3|\mathbf{L}|}{2}\ln(2\pi)-\frac{1}{2}\ln\left\{\det\left(\boldsymbol{I}+\sigma^2\sum_{\kappa\in\mathbf{K}}\sum_{\kappa'\in\mathbf{K}}\alpha_{\kappa,\kappa'}\boldsymbol{C}(\kappa,\kappa')^{\nu}\right)\right\}+\frac{1}{2}\ln\left\{\det\left(\sum_{\kappa\in\mathbf{K}}\sum_{\kappa'\in\mathbf{K}}\alpha_{\kappa,\kappa'}\boldsymbol{C}(\kappa,\kappa')^{\nu}\right)\right\}$$
$$-\frac{1}{2}\boldsymbol{g}^T\left(\sum_{\kappa\in\mathbf{K}}\sum_{\kappa'\in\mathbf{K}}\alpha_{\kappa,\kappa'}\boldsymbol{C}(\kappa,\kappa')^{\nu}\right)\left(\boldsymbol{I}+\sigma^2\sum_{\kappa\in\mathbf{K}}\sum_{\kappa'\in\mathbf{K}}\alpha_{\kappa,\kappa'}\boldsymbol{C}(\kappa,\kappa')^{\nu}\right)^{-1}\boldsymbol{g}$$
$$=-\frac{3|\mathbf{L}|}{2}\ln(2\pi)-\frac{1}{2}\sum_{(p,q)\in\mathbf{L}}\ln\{\det[\boldsymbol{e}+\sigma^2\lambda(p,q)^{\nu}\boldsymbol{\alpha}]\}+\frac{1}{2}\sum_{(p,q)\in\mathbf{L}}\ln\{\det[\lambda(p,q)^{\nu}\boldsymbol{\alpha}]\}$$
$$-\frac{1}{2}\sum_{(p,q)\in\mathbf{L}}\vec{G}^{\dagger}(p,q)\lambda(p,q)^{\nu}\boldsymbol{\alpha}[\boldsymbol{e}+\sigma^2\lambda(p,q)^{\nu}\boldsymbol{\alpha}]^{-1}\vec{G}(p,q). \tag{2.27}$$

By replacing the summation $1/|\mathbf{L}|\Sigma_{(p,q)\in\mathbf{L}}$ by the integral $1/4\pi^2\int_0^{2\pi}d\theta\int_0^{2\pi}d\phi$, the third term in the right-hand side of Eq. (2.27) can be rewritten as follows:

$$\frac{1}{2|\mathbf{L}|}\sum_{(p,q)\in\mathbf{L}}\ln\{\det[\lambda(p,q)^{\nu}\boldsymbol{\alpha}]\}$$
$$=\frac{3\nu}{2|\mathbf{L}|}\sum_{(p,q)\in\mathbf{L}}\ln[\lambda(p,q)]+\frac{1}{2}\ln[\det(\boldsymbol{\alpha})]$$
$$=\frac{3\nu}{8\pi^2}\int_0^{2\pi}\int_0^{2\pi}\ln\left(1-\frac{1}{2}\cos\theta-\frac{1}{2}\cos\phi\right)d\theta d\phi+\frac{1}{2}\ln[\det(\boldsymbol{\alpha})]$$
$$=-3\nu\ln(2)+\frac{12\nu\chi}{\pi}+\frac{1}{2}\ln[\det(\boldsymbol{\alpha})], \tag{2.28}$$

where χ is the Catalan constant, namely, $\chi=0.915\,96\ldots$. For a fixed value of ν, the conditions for an extremum of $\Pr\{\boldsymbol{G}=\boldsymbol{g}|\boldsymbol{\alpha},\nu,\sigma\}$ at $\boldsymbol{\alpha}=\hat{\boldsymbol{\alpha}}$ and $\sigma=\hat{\sigma}$ can be reduced to the following simultaneous equations:

$$\hat{\boldsymbol{\alpha}}^{-1}=\frac{1}{|\mathbf{L}|}\sum_{(p,q)\in\mathbf{L}}\{\lambda(p,q)^{\nu}[\boldsymbol{e}+\hat{\sigma}^2\lambda(p,q)^{\nu}\hat{\boldsymbol{\alpha}}]^{-1}\}$$
$$+\frac{1}{|\mathbf{L}|}\sum_{(p,q)\in\mathbf{L}}\vec{G}^{\dagger}(p,q)\left[\frac{\partial}{\partial\alpha_{\kappa,\kappa'}}\{\lambda(p,q)^{\nu}\times\boldsymbol{\alpha}[\boldsymbol{e}+\hat{\sigma}^2\lambda(p,q)^{\nu}\boldsymbol{\alpha}]^{-1}\}\right]_{\boldsymbol{\alpha}=\hat{\boldsymbol{\alpha}}}\vec{G}(p,q), \tag{2.29}$$

$$\hat{\sigma}^2=\frac{1}{3|\mathbf{L}|}\sum_{(p,q)\in\mathbf{L}}\mathrm{tr}\{\hat{\sigma}^2[\boldsymbol{e}+\hat{\sigma}^2\lambda(p,q)^{\nu}\hat{\boldsymbol{\alpha}}]^{-1}\}$$
$$+\frac{1}{3|\mathbf{L}|}\sum_{(p,q)\in\mathbf{L}}\vec{G}^{\dagger}(p,q)\{\hat{\sigma}^4\lambda(p,q)^{2\nu}\times\hat{\boldsymbol{\alpha}}^2[\boldsymbol{e}+\hat{\sigma}^2\lambda(p,q)^{\nu}\hat{\boldsymbol{\alpha}}]^{-2}\}\vec{G}(p,q). \tag{2.30}$$

The restored image $\hat{\boldsymbol{f}}$ in Eq. (2.15) can be expressed as follows:

$$\hat{\boldsymbol{f}}=\left(\boldsymbol{I}+\hat{\sigma}^2\sum_{\kappa\in\mathbf{K}}\sum_{\kappa'\in\mathbf{K}}\hat{\alpha}_{\kappa,\kappa'}\boldsymbol{C}(\kappa,\kappa')^{\hat{\nu}}\right)^{-1}\boldsymbol{g}, \tag{2.31}$$

so that we have

$$\begin{pmatrix}\hat{f}_{x,y,\text{red}}\\ \hat{f}_{x,y,\text{green}}\\ \hat{f}_{x,y,\text{blue}}\end{pmatrix}=\frac{1}{|\mathbf{L}|}\sum_{(p,q)\in\mathbf{L}}[\boldsymbol{e}+\hat{\sigma}^2\lambda(p,q)^{\hat{\nu}}\hat{\boldsymbol{\alpha}}]^{-1}\times\left[\cos\left(\frac{2\pi px}{L_x}+\frac{2\pi qy}{L_y}\right)\mathrm{Re}\,\vec{G}(p,q)+\sin\left(\frac{2\pi px}{L_x}+\frac{2\pi qy}{L_y}\right)\mathrm{Im}\,\vec{G}(p,q)\right]. \tag{2.32}$$

III. NUMERICAL EXPERIMENTS

In this section, we give some numerical experiments for the original images given in Fig. 1. In the numerical experiments, we treat the full color digital images with 24 bits as the original and the degraded images. The value of hyperparameter σ set in producing the degraded image $\boldsymbol{g}$ in an additive white Gaussian noise $\mathcal{N}[0,\sigma^2]$ is denoted by the notation σ^*. The degraded images $\boldsymbol{g}$ produced from the original images $\boldsymbol{f}$ by setting $\sigma^*=40$ in the degradation process (2.1) are shown in Figs. 2(b) and 3(b).

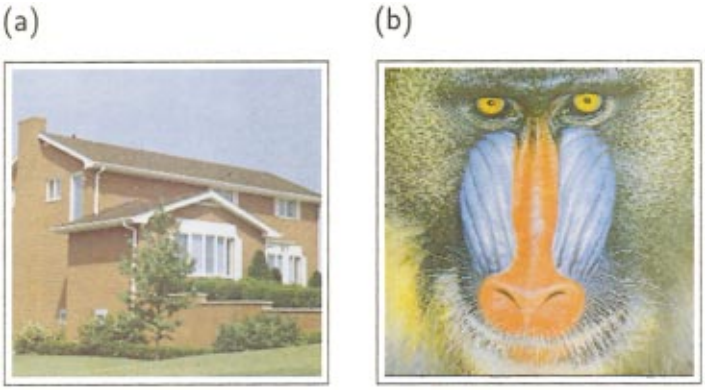

FIG. 1. (Color) Original images. (a) Home. (b) Mandrill.

The estimates of hyperparameters $\hat{\boldsymbol{\alpha}}$, $\hat{\nu}$, and $\hat{\sigma}$ are determined so as to maximize the logarithm of evidence, $\ln(\Pr\{\boldsymbol{G}=\boldsymbol{g}|\boldsymbol{\alpha},\nu,\sigma\})$, given by Eq. (2.27) and the restored image $\hat{\boldsymbol{f}}$ is obtained by using Eq. (2.32). For a fixed value of ν, the practical algorithm for calculating

$$[\hat{\boldsymbol{\alpha}}(\nu),\hat{\sigma}(\nu)]=\arg\max_{(\boldsymbol{\alpha},\sigma)}\Pr\{\boldsymbol{G}=\boldsymbol{g}|\boldsymbol{\alpha},\nu,\sigma\} \tag{3.1}$$

is given as follows.

Step 1. Calculate the discrete Fourier transform $\vec{G}(p,q)$ of the given degraded image $\boldsymbol{g}$ by means of Eq. (2.25). Set $r\leftarrow 0$,

$$\boldsymbol{a}(0)\leftarrow\begin{pmatrix} 1 & \frac{1}{2} & \frac{1}{2} \\ \frac{1}{2} & 1 & \frac{1}{2} \\ \frac{1}{2} & \frac{1}{2} & 1 \end{pmatrix}$$

and $b(0)\leftarrow 1$.

Step 2. Update $r\leftarrow r+1$; and

$$\boldsymbol{a}(r)\equiv\begin{pmatrix} a_{\mathrm{red,red}}(r) & a_{\mathrm{red,green}}(r) & a_{\mathrm{red,blue}}(r) \\ \alpha_{\mathrm{green,red}}(r) & a_{\mathrm{green,green}}(r) & a_{\mathrm{green,blue}}(r) \\ \alpha_{\mathrm{blue,red}}(r) & a_{\mathrm{blue,green}}(r) & a_{\mathrm{blue,blue}}(r) \end{pmatrix}$$

$$\leftarrow\Bigg(\frac{1}{|\mathbf{L}|}\sum_{(p,q)\in\mathbf{L}}\{\lambda(p,q)^{\nu}[b(r-1)\boldsymbol{e}+\lambda(p,q)^{\nu}\times\boldsymbol{a}(r-1)]^{-1}\}+\frac{1}{|\mathbf{L}|}\sum_{(p,q)\in\mathbf{L}}\vec{G}^{\dagger}(p,q)\times\Bigg[\frac{\partial}{\partial\boldsymbol{\alpha}}\{b(r-1)\lambda(p,q)^{\nu}\boldsymbol{\alpha}[b(r-1)\boldsymbol{e}$$

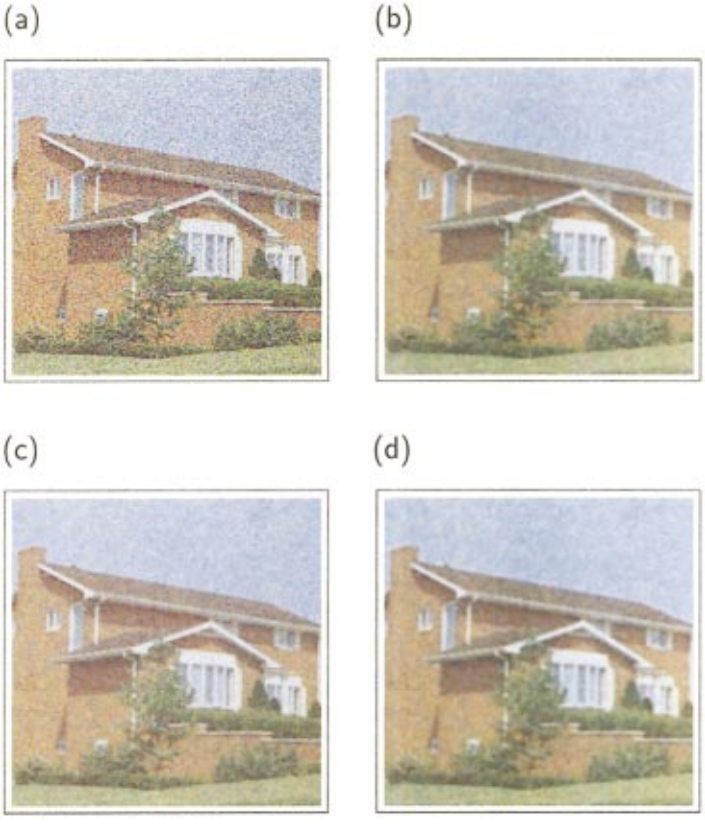

FIG. 2. (Color) Image restoration. (a) Degraded image $\boldsymbol{g}$ generated from the original image $\boldsymbol{f}$ in Fig. 1(a) by the additive white Gaussian noise $\mathcal{N}[0,40^2]$. (b) Restored image $\hat{\boldsymbol{f}}$ for the proposed model. (c) Restored image $\hat{\boldsymbol{f}}$ for the multichannel CAR model ($\nu=1$). (d) Restored image $\hat{\boldsymbol{f}}$ for the multichannel SAR model ($\nu=2$).

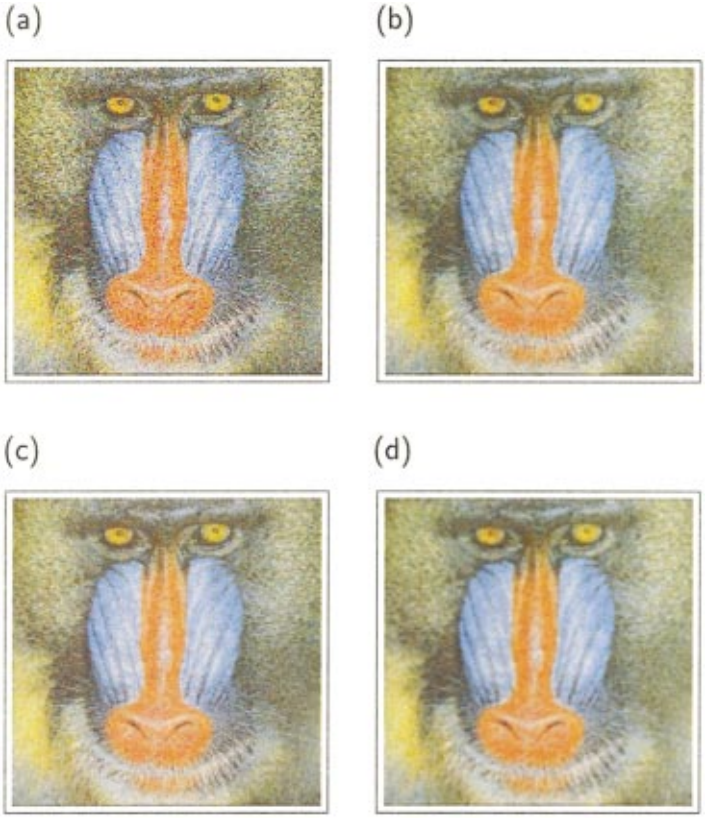

FIG. 3. (Color) Image restoration. (a) Degraded image $\boldsymbol{g}$ generated from the original image $\boldsymbol{f}$ in Fig. 1(b) by the additive white Gaussian noise $\mathcal{N}[0,40^2]$. (b) Restored image $\hat{\boldsymbol{f}}$ for the proposed model. (c) Restored image $\hat{\boldsymbol{f}}$ for the multichannel CAR model ($\nu=1$). (d) Restored image $\hat{\boldsymbol{f}}$ for the multichannel SAR model ($\nu=2$).

$$+\lambda(p,q)^{\nu}\boldsymbol{\alpha}]^{-1}\}\Big]_{\boldsymbol{\alpha}=\boldsymbol{a}(r-1)}\vec{G}(p,q)\Bigg)^{-1}, \tag{3.2}$$

$$b(r)\leftarrow\frac{1}{|\mathbf{L}|}\sum_{(p,q)\in\mathbf{L}}\mathrm{tr}\{[b(r-1)\boldsymbol{e}+\lambda(p,q)^{\nu}\boldsymbol{a}(r-1)]^{-1}\}$$
$$+\frac{1}{|\mathbf{L}|}\sum_{(p,q)\in\mathbf{L}}\vec{G}^{\dagger}(p,q)\lambda(p,q)^{2\nu}\boldsymbol{a}(r-1)^2$$
$$\times[b(r-1)\boldsymbol{e}+\lambda(p,q)^{\nu}\boldsymbol{a}(r-1)]^{-2}\vec{G}(p,q), \tag{3.3}$$

$$c(r)\leftarrow-\frac{3|\mathbf{L}|}{2}\ln(2\pi)-\frac{1}{2}\sum_{(p,q)\in\mathbf{L}}\ln\{\det[\boldsymbol{e}+b(r)$$
$$\times\lambda(p,q)^{\nu}\boldsymbol{a}(r)]\}-3\nu\ln 2+\frac{12\nu\chi}{\pi}$$
$$+\frac{1}{2}\ln\{\det[\boldsymbol{a}(r)]\}-\frac{1}{2}\sum_{(p,q)\in\mathbf{L}}\vec{G}^{\dagger}(p,q)\lambda(p,q)^{\nu}$$
$$\times\boldsymbol{\alpha}[\boldsymbol{e}+b(r)\lambda(p,q)^{\nu}\boldsymbol{a}(r)]^{-1}\vec{G}(p,q). \tag{3.4}$$

Step 3. Update $\hat{\sigma}(\nu)\leftarrow\sqrt{b(r)}$, $\hat{\boldsymbol{\alpha}}(\nu)\leftarrow\boldsymbol{a}(r)$, and $R\leftarrow r$. Stop if it is satisfied that

$$\varepsilon(r)\equiv\sum_{\kappa=\mathrm{red,green,blue}}\sum_{\kappa'=\mathrm{red,green,blue}}\left|\frac{a_{\kappa,\kappa'}(r)-a_{\kappa,\kappa'}(r-1)}{a_{\kappa,\kappa'}(r-1)}\right|$$
$$+\left|\frac{b(r)-b(r-1)}{b(r-1)}\right|<10^{-4}, \tag{3.5}$$

and go to step 2 otherwise.

The logarithm of evidence $\ln\rho\{\boldsymbol{G}=\boldsymbol{g}|\hat{\boldsymbol{\alpha}}(\nu),\nu,\hat{\sigma}(\nu)\}$ is obtained by using the following substitution:

$$\mathcal{L}(\boldsymbol{g},\hat{\boldsymbol{\alpha}}(\nu),\nu,\hat{\sigma}(\nu))\equiv\frac{1}{|\mathbf{L}|}\ln\rho\{\boldsymbol{G}=\boldsymbol{g}|\hat{\boldsymbol{\alpha}}(\nu),\nu,\hat{\sigma}(\nu)\}\leftarrow c(R). \tag{3.6}$$

The convergence behavior of $\varepsilon(r)$ in Eq. (3.5) and the one of $c(r)$ in Eq. (3.4) are given in Figs. 4 and 5 for the degraded images $\boldsymbol{g}$ given in Figs. 2(a) and 3(a) by setting $\nu=1.356\,00$. The behavior of $\varepsilon(r)$ shows the convergence of $\boldsymbol{a}(r)$ and $b(r)$ in the iterative procedure and the one of $c(r)$ suggests the achievement of the maximization of the logarithm of evidence in the iterative procedure. We have also checked numerically that the iteration procedure converges to the same values irrespective of some different choices in the initial values $\boldsymbol{a}(0)$ and $b(0)$ in the step 1 of the above algorithm. Moreover, for various values of hyperparameters $\boldsymbol{\alpha}$ and σ, the values of $\mathcal{L}(\boldsymbol{g},\boldsymbol{\alpha},\nu,\sigma)$ calculated for the degraded image $\boldsymbol{g}$ in Fig. 2(a) are given in Tables I and II. Tables I and II show us the uniqueness of the maximum point of the evidence with respect to $\boldsymbol{\alpha}$ and σ for a fixed value of ν. There are many choices for halting criterion in the above algorithm. In the present paper, we choose the simplest choice, because the same results for some different choices in numerical experiments are obtained for a degraded image $\boldsymbol{g}$. We check not only Eq. (3.5) but also the following criteria:

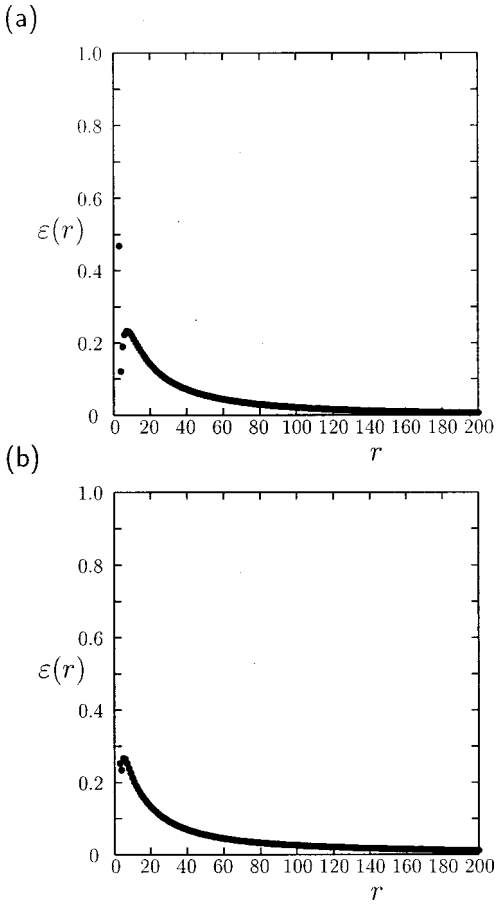

FIG. 4. Convergence of $\varepsilon(r)$ in the iterative process for the degraded image $\boldsymbol{g}$ given in Figs. 2(a) and 3(a). (a) Home ($\nu = 1.356\,00$). (b) Mandrill ($\nu = 1.017\,00$).

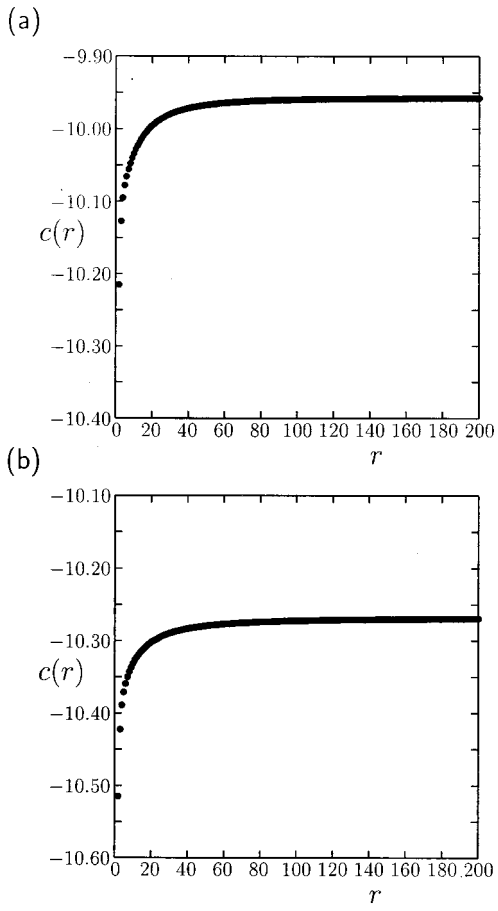

FIG. 5. Convergence of $c(r)$ in the iterative process for the degraded image $\boldsymbol{g}$ given in Figs. 2(a) and 3(a). (a) Home ($\nu = 1.356\,00$). (b) Mandrill ($\nu = 1.017\,00$).

$$\sum_{\kappa=\text{red,green,blue}} \sum_{\kappa'=\text{red,green,blue}} [a_{\kappa,\kappa'}(r)-a_{\kappa,\kappa'}(r-1)]^2 + [b(r)-b(r-1)]^2 < 10^{-4}, \tag{3.7}$$

$$\left|\frac{c(r)-c(r-1)}{c(r)}\right| < 10^{-4}, \tag{3.8}$$

and

$$[c(r)-c(r-1)]^2 < 10^{-4}. \tag{3.9}$$

The number of iterations is the similar order as R for Eq. (3.5). In order to show the convergence of the iterative procedure (3.2) and (3.3), we give in Table III values of $\hat{\sigma}(\nu)$, $\hat{\boldsymbol{\alpha}}(\nu)$, $\mathcal{L}(\boldsymbol{g},\hat{\boldsymbol{\alpha}}(\nu),\nu,\hat{\sigma}(\nu))$, and R, which are obtained by applying the above practical algorithm for various values of ν to the degraded image $\boldsymbol{g}$ given in Fig. 2(b). We check numerically that the logarithm of evidence, $\mathcal{L}(\boldsymbol{g},\boldsymbol{\alpha},\nu,\sigma)$, has a unique maximum value with respect to various values of σ, ν, and $\boldsymbol{\alpha}$ for each degraded image $\boldsymbol{g}$ as shown in Tables I–III. In the proposed model, the estimates of hyperparameters, $\hat{\boldsymbol{\alpha}}$, $\hat{\sigma}$, and $\hat{\nu}$ are obtained by using the following substitution:

$$\hat{\boldsymbol{\alpha}} \leftarrow \hat{\boldsymbol{\alpha}}(\hat{\nu}), \quad \hat{\sigma} \leftarrow \hat{\sigma}(\hat{\nu}), \tag{3.10}$$

where

$$\hat{\nu} \leftarrow \arg\max_{\nu} \Pr\{\boldsymbol{G}=\boldsymbol{g}|\hat{\boldsymbol{\alpha}}(\nu),\nu,\hat{\sigma}(\nu)\}. \tag{3.11}$$

In the numerical experiments, we calculate the values of $\hat{\boldsymbol{\alpha}}(\nu)$ and $\hat{\sigma}(\nu)$ by means of the above algorithm for various values of ν and determine the $\hat{\nu}$ so as to maximize the logarithm of evidence, $\mathcal{L}(\boldsymbol{g},\hat{\boldsymbol{\alpha}}(\nu),\nu,\sigma(\nu))$, defined by Eq. (3.6). The evaluation of the value $\hat{\nu}$ in this procedure is explicitly shown in Table III. For the obtained estimates $\hat{\boldsymbol{\alpha}}$, $\hat{\nu}$, and $\hat{\sigma}$, the restored image $\hat{\boldsymbol{f}} \equiv \{\hat{f}_{x,y,\kappa}\}$ is determined by

$$\hat{f}_{x,y,\kappa} \leftarrow \arg\min_{n=0,1,\ldots,255} \left(n - \int z_{x,y,\kappa} \times \Pr\{\boldsymbol{F}=\boldsymbol{z}|\boldsymbol{G}=\boldsymbol{g},\hat{\boldsymbol{\alpha}},\hat{\nu},\hat{\sigma}\} d\boldsymbol{z} \right)^2. \tag{3.12}$$

The estimation of the restored image $\hat{\boldsymbol{f}}$ in Eq. (3.12) is called thresholded posterior mean estimation [12,19,20]. The inte-

TABLE I. Values of $\mathcal{L}(\boldsymbol{g},\boldsymbol{\alpha},\nu,\sigma)$ obtained for various values of $\alpha_{\mathrm{red,red}}$, $\alpha_{\mathrm{red,green}}$, $\alpha_{\mathrm{red,blue}}$, and σ in the degraded image $\boldsymbol{g}$ given in Fig. 2(a) when we set $\nu=1.356\,00$.

(a) $\alpha_{\mathrm{green,green}}=0.03452$, $\alpha_{\mathrm{blue,blue}}=0.02752$, $\alpha_{\mathrm{red,green}}=\alpha_{\mathrm{green,red}}=-0.01495$, $\alpha_{\mathrm{red,blue}}=\alpha_{\mathrm{blue,red}}=0.00090$, $\alpha_{\mathrm{green,blue}}=\alpha_{\mathrm{blue,green}}=-0.02318$

	$\alpha_{\mathrm{red,red}}=0.018$	$\alpha_{\mathrm{red,red}}=0.019$	$\alpha_{\mathrm{red,red}}=0.020$	$\alpha_{\mathrm{red,red}}=0.021$	$\alpha_{\mathrm{red,red}}=0.022$	$\alpha_{\mathrm{red,red}}=0.023$	$\alpha_{\mathrm{red,red}}=0.024$
$\sigma=30$	−10.077	−10.084	−10.092	−10.100	−10.108	−10.116	−10.123
$\sigma=35$	−9.969	−9.969	−9.971	−9.974	−9.977	−9.981	−9.984
$\sigma=40$	−9.971	−9.967	−9.966	−9.966	−9.967	−9.968	−9.969
$\sigma=45$	−10.035	−10.029	−10.026	−10.024	−10.023	−10.023	−10.023
$\sigma=50$	−10.133	−10.126	−10.122	−10.119	−10.117	−10.116	−10.115

(b) $\alpha_{\mathrm{red,red}}=0.01951$, $\alpha_{\mathrm{green,green}}=0.03452$, $\alpha_{\mathrm{blue,blue}}=0.02752$, $\alpha_{\mathrm{green,red}}=-0.01495$, $\alpha_{\mathrm{red,blue}}=\alpha_{\mathrm{blue,red}}=0.00090$, $\alpha_{\mathrm{green,blue}}=\alpha_{\mathrm{blue,green}}=-0.02318$

	$\alpha_{\mathrm{red,green}}=-0.017$	$\alpha_{\mathrm{red,green}}=-0.016$	$\alpha_{\mathrm{red,green}}=-0.015$	$\alpha_{\mathrm{red,green}}=-0.014$	$\alpha_{\mathrm{red,green}}=-0.013$	$\alpha_{\mathrm{red,green}}=-0.012$	$\alpha_{\mathrm{red,green}}=-0.011$
$\sigma=30$	−10.074	−10.079	−10.087	−10.096	−10.107	−10.117	−10.127
$\sigma=35$	−9.971	−9.969	−9.970	−9.972	−9.977	−9.981	−9.986
$\sigma=40$	−9.977	−9.970	−9.967	−9.966	−9.966	−9.968	−9.970
$\sigma=45$	−10.042	−10.033	−10.027	−10.024	−10.023	−10.023	−10.023
$\sigma=50$	−10.141	−10.130	−10.124	−10.120	−10.117	−10.116	−10.115

(c) $\alpha_{\mathrm{red,red}}=0.01951$, $\alpha_{\mathrm{green,green}}=0.03452$, $\alpha_{\mathrm{blue,blue}}=0.02752$, $\alpha_{\mathrm{red,green}}=\alpha_{\mathrm{green,red}}=-0.01495$, $\alpha_{\mathrm{blue,red}}=0.00090$, $\alpha_{\mathrm{green,blue}}=\alpha_{\mathrm{blue,green}}=-0.02318$

	$\alpha_{\mathrm{red,blue}}=-0.001$	$\alpha_{\mathrm{red,blue}}=0.000$	$\alpha_{\mathrm{red,blue}}=0.001$	$\alpha_{\mathrm{red,blue}}=0.002$	$\alpha_{\mathrm{red,blue}}=0.003$	$\alpha_{\mathrm{red,blue}}=0.004$	$\alpha_{\mathrm{red,blue}}=0.005$
$\sigma=30$	−10.076	−10.081	−10.088	−10.096	−10.105	−10.114	−10.123
$\sigma=35$	−9.970	−9.969	−9.970	−9.972	−9.976	−9.980	−9.984
$\sigma=40$	−9.973	−9.968	−9.966	−9.966	−9.966	−9.968	−9.969
$\sigma=45$	−10.037	−10.031	−10.027	−10.024	−10.023	−10.023	−10.023
$\sigma=50$	−10.136	−10.128	−10.123	−10.120	−10.118	−10.116	−10.116

grand of $\int z_{x,y,\kappa}\Pr\{\boldsymbol{F}=\boldsymbol{z}|\boldsymbol{G}=\boldsymbol{g},\hat{\boldsymbol{\alpha}},\hat{\nu},\hat{\sigma}\}d\boldsymbol{z}$ is calculated by means of the right-hand side of Eq. (2.32) in Eq. (2.21). In the CAR and the SAR model, the hyperparameter ν should be set to 1 and 2, respectively. The estimates of hyperparameters, $\hat{\alpha}$ and $\hat{\sigma}$, are obtained by using the following substitution:

$$\hat{\nu}\leftarrow 1,\quad \hat{\boldsymbol{\alpha}}\leftarrow\hat{\boldsymbol{\alpha}}(1),\quad \hat{\sigma}\leftarrow\hat{\sigma}(1)\quad (\text{CAR model}), \tag{3.13}$$

and

$$\hat{\nu}\leftarrow 2,\quad \hat{\boldsymbol{\alpha}}\leftarrow\hat{\boldsymbol{\alpha}}(2),\quad \hat{\sigma}\leftarrow\hat{\sigma}(2)\quad (\text{SAR model}), \tag{3.14}$$

for the CAR and the SAR model, respectively.

For the degraded images $\boldsymbol{g}$ obtained from the original images $\boldsymbol{f}$ in Fig. 1 by setting $\sigma^*=30$, 40, and 50 in the degradation process (2.1), the estimated values of hyperparameters $\hat{\boldsymbol{\alpha}}$, $\hat{\nu}$, and $\hat{\sigma}$ and the values of

$$\mathcal{E}(\boldsymbol{f},\hat{\boldsymbol{f}})\equiv\frac{1}{3|\mathbf{L}|}||\boldsymbol{f}-\hat{\boldsymbol{f}}||^2$$

and

$$\Delta_{\mathrm{SNR}}\equiv 10\log_{10}\left(\frac{||\boldsymbol{f}-\boldsymbol{g}||^2}{||\boldsymbol{f}-\hat{\boldsymbol{f}}||^2}\right)\ (\mathrm{dB})$$

are given in Table IV. For the case of the CAR model ($\nu=1$) and the SAR model ($\nu=2$), the estimated values of hyperparameters $\hat{\alpha}$ and $\hat{\sigma}$ and the values of $\mathcal{E}(\boldsymbol{f},\hat{\boldsymbol{f}})$ and Δ_{SNR} are given in Tables V and VI, respectively. The degraded images $\boldsymbol{g}$ and the restored image $\hat{\boldsymbol{f}}$ for the original image $\boldsymbol{f}$ in $\sigma^*=40$ are given in Figs. 2 and 3.

Before closing this section, we give a comparison between the present method and a familiar technique of filter theory in image processing. As one of familiar methods of filter theory, we have a constrained least squares filter. We assume that the degradation process is the additive white

TABLE II. Values of $\mathcal{L}(\boldsymbol{g},\boldsymbol{\alpha},\nu,\sigma)$ obtained for various values of $\alpha_{\mathrm{green,green}}$, $\alpha_{\mathrm{green,blue}}$, $\alpha_{\mathrm{blue,blue}}$, and σ in the degraded image $\boldsymbol{g}$ given in Fig. 2(a) when we set $\nu=1.356\,00$.

(a) $\alpha_{\mathrm{red,red}}=0.01951$, $\alpha_{\mathrm{blue,blue}}=0.02752$, $\alpha_{\mathrm{red,green}}=\alpha_{\mathrm{green,red}}=-0.01495$, $\alpha_{\mathrm{red,blue}}=\alpha_{\mathrm{blue,red}}=0.00090$, $\alpha_{\mathrm{green,blue}}=\alpha_{\mathrm{blue,green}}=-0.02318$

	$\alpha_{\mathrm{green,green}}=0.032$	$\alpha_{\mathrm{green,green}}=0.033$	$\alpha_{\mathrm{green,green}}=0.034$	$\alpha_{\mathrm{green,green}}=0.035$	$\alpha_{\mathrm{green,green}}=0.036$	$\alpha_{\mathrm{green,green}}=0.037$	$\alpha_{\mathrm{green,green}}=0.038$
$\sigma=30$	−10.080	−10.075	−10.082	−10.093	−10.105	−10.117	−10.129
$\sigma=35$	−9.987	−9.971	−9.969	−9.971	−9.976	−9.982	−9.987
$\sigma=40$	−9.998	−9.976	−9.968	−9.966	−9.966	−9.968	−9.971
$\sigma=45$	−10.066	−10.041	−10.030	−10.025	−10.023	−10.023	−10.024
$\sigma=50$	−10.167	−10.140	−10.127	−10.121	−10.118	−10.116	−10.116

(b) $\alpha_{\mathrm{red,red}}=0.01951$, $\alpha_{\mathrm{green,green}}=0.03452$, $\alpha_{\mathrm{blue,blue}}=0.02752$, $\alpha_{\mathrm{red,green}}=\alpha_{\mathrm{green,red}}=-0.01495$, $\alpha_{\mathrm{red,blue}}=\alpha_{\mathrm{blue,red}}=0.00090$, $\alpha_{\mathrm{blue,green}}=-0.02318$

	$\alpha_{\mathrm{green,blue}}=-0.025$	$\alpha_{\mathrm{green,blue}}=-0.024$	$\alpha_{\mathrm{green,blue}}=-0.023$	$\alpha_{\mathrm{green,blue}}=-0.022$	$\alpha_{\mathrm{green,blue}}=-0.021$	$\alpha_{\mathrm{green,blue}}=-0.020$	$\alpha_{\mathrm{green,blue}}=-0.019$
$\sigma=30$	−10.075	−10.080	−10.089	−10.100	−10.111	−10.122	−10.133
$\sigma=35$	−9.971	−9.969	−9.970	−9.974	−9.979	−9.984	−9.990
$\sigma=40$	−9.976	−9.969	−9.966	−9.966	−9.967	−9.969	−9.972
$\sigma=45$	−10.041	−10.031	−10.026	−10.024	−10.023	−10.023	−10.024
$\sigma=50$	−10.140	−10.129	−10.123	−10.119	−10.117	−10.116	−10.116

(c) $\alpha_{\mathrm{red,red}}=0.01951$, $\alpha_{\mathrm{green,green}}=0.03452$, $\alpha_{\mathrm{red,green}}=\alpha_{\mathrm{green,red}}=-0.01495$, $\alpha_{\mathrm{red,blue}}=\alpha_{\mathrm{blue,red}}=0.00090$, $\alpha_{\mathrm{green,blue}}=\alpha_{\mathrm{green,blue}}=-0.02318$

	$\alpha_{\mathrm{blue,blue}}=0.025$	$\alpha_{\mathrm{blue,blue}}=0.026$	$\alpha_{\mathrm{blue,blue}}=0.027$	$\alpha_{\mathrm{blue,blue}}=0.028$	$\alpha_{\mathrm{blue,blue}}=0.029$	$\alpha_{\mathrm{blue,blue}}=0.030$	$\alpha_{\mathrm{blue,blue}}=0.031$
$\sigma=30$	−10.076	−10.076	−10.083	−10.092	−10.101	−10.111	−10.120
$\sigma=35$	−9.977	−9.970	−9.970	−9.971	−9.974	−9.978	−9.983
$\sigma=40$	−9.985	−9.973	−9.968	−9.966	−9.966	−9.967	−9.969
$\sigma=45$	−10.052	−10.037	−10.029	−10.025	−10.024	−10.023	−10.023
$\sigma=50$	−10.151	−10.135	−10.126	−10.121	−10.119	−10.117	−10.116

Gaussian noise in Eq. (2.1). When a degraded image $\boldsymbol{g}$ is given, the constrained least squares filter [23] is formulated in the RGB space as follows:

$$\hat{\boldsymbol{f}}=\arg\min_{\boldsymbol{z}:||\boldsymbol{z}-\boldsymbol{g}||_{\kappa}^{2}=|\mathbf{L}|\sigma^{*2}\ (\kappa\in\mathbf{K})}\left(\sum_{\kappa\in\mathbf{K}}||\boldsymbol{C}(\kappa,\kappa)\boldsymbol{z}||^{2}\right), \tag{3.15}$$

where

$$||\boldsymbol{z}-\boldsymbol{g}||_{\kappa}^{2}\equiv\sum_{(x,y)\in\mathbf{L}}(z_{x,y,\kappa}-g_{x,y,\kappa})^{2}. \tag{3.16}$$

By introduce Lagrange multipliers γ_{κ} to ensure the constrained condition $||\boldsymbol{z}-\boldsymbol{g}||_{\kappa}^{2}=|\mathbf{L}|\sigma^{*2}$ and applying the discrete Fourier transform to the matrix $\boldsymbol{C}(\kappa,\kappa)$, we have

$$\begin{pmatrix}\hat{f}_{x,y,\mathrm{red}}\\ \hat{f}_{x,y,\mathrm{green}}\\ \hat{f}_{x,y,\mathrm{blue}}\end{pmatrix}=\frac{1}{|\mathbf{L}|}\sum_{(p,q)\in\mathbf{L}}\begin{pmatrix}\frac{1}{1+\gamma_{\mathrm{red}}\lambda(p,q)^{2}} & 0 & 0\\ 0 & \frac{1}{1+\gamma_{\mathrm{green}}\lambda(p,q)^{2}} & 0\\ 0 & 0 & \frac{1}{1+\gamma_{\mathrm{blue}}\lambda(p,q)^{2}}\end{pmatrix}\times\left[\cos\left(\frac{2\pi px}{L_x}+\frac{2\pi qy}{L_y}\right)\mathrm{Re}\,\vec{G}(p,q)+\sin\left(\frac{2\pi px}{L_x}+\frac{2\pi qy}{L_y}\right)\mathrm{Im}\,\vec{G}(p,q)\right]. \tag{3.17}$$

TABLE III. Values of $\hat{\sigma}(\nu)$, $\hat{\boldsymbol{\alpha}}(\nu)$, $\mathcal{L}(\boldsymbol{g},\hat{\boldsymbol{\alpha}}(\nu),\nu,\hat{\sigma}(\nu))$, and R obtained for various values of ν in the degraded image $\boldsymbol{g}$ given in Fig. 2(a). Here, R is the number of iterations in the proposed algorithm.

ν	$\hat{\sigma}(\nu)$	$\hat{\boldsymbol{\alpha}}(\nu)=\begin{pmatrix} \hat{\alpha}_{\mathrm{red,red}} & \hat{\alpha}_{\mathrm{red,green}} & \hat{\alpha}_{\mathrm{red,blue}} \\ \hat{\alpha}_{\mathrm{green,red}} & \hat{\alpha}_{\mathrm{green,green}} & \hat{\alpha}_{\mathrm{green,blue}} \\ \hat{\alpha}_{\mathrm{blue,red}} & \hat{\alpha}_{\mathrm{blue,green}} & \hat{\alpha}_{\mathrm{blue,blue}} \end{pmatrix}$	$\mathcal{L}(\boldsymbol{g},\hat{\boldsymbol{\alpha}}(\nu),\nu,\hat{\sigma}(\nu))$	R
1.0	35.637	$\begin{pmatrix} 0.00514 & -0.00269 & -0.00057 \\ -0.00269 & 0.00708 & -0.00420 \\ -0.00057 & -0.00420 & 0.00654 \end{pmatrix}$	−9.96675	376
1.2	36.953	$\begin{pmatrix} 0.01079 & -0.00722 & -0.00025 \\ -0.00722 & 0.01734 & -0.01123 \\ -0.00025 & -0.01123 & 0.01464 \end{pmatrix}$	−9.95913	523
1.3560	37.570	$\begin{pmatrix} 0.01951 & -0.01495 & 0.00090 \\ -0.01495 & 0.03452 & -0.02318 \\ 0.00090 & -0.02318 & 0.02752 \end{pmatrix}$	−9.95767	653
1.4	37.713	$\begin{pmatrix} 0.02310 & -0.01829 & 0.00153 \\ -0.01829 & 0.04193 & -0.02837 \\ 0.00153 & -0.02837 & 0.03295 \end{pmatrix}$	−9.95777	692
1.6	38.253	$\begin{pmatrix} 0.05063 & -0.04548 & 0.00800 \\ -0.04548 & 0.10224 & -0.07092 \\ 0.00800 & -0.07092 & 0.07572 \end{pmatrix}$	−9.96030	883
1.8	38.677	$\begin{pmatrix} 0.11355 & -0.11331 & 0.02881 \\ -0.11331 & 0.25364 & -0.17874 \\ 0.02881 & -0.17874 & 0.17888 \end{pmatrix}$	−9.96525	1093
2.0	39.029	$\begin{pmatrix} 0.26091 & -0.28542 & 0.09199 \\ -0.28542 & 0.64120 & -0.45685 \\ 0.09199 & -0.45685 & 0.43440 \end{pmatrix}$	−9.97166	1320

The Lagrange multipliers γ_κ are determined so as to satisfy the following equations:

$$\gamma_\kappa=\frac{\sigma^{*2}}{\dfrac{1}{|\mathbf{L}|}\displaystyle\sum_{(p,q)\in\mathbf{L}}|G_\kappa(p,q)|^2\frac{\lambda(p,q)^4}{[1+\gamma_\kappa\lambda(p,q)^2]^2}}[\kappa\in\mathbf{K}]. \tag{3.18}$$

For the degraded images $\boldsymbol{g}$ obtained from the original images $\boldsymbol{f}$ in Fig. 1 by setting $\sigma^*=30$, 40 and 50 in the degradation process (2.1), the estimated values of Lagrange multipliers γ_{red}, γ_{green}, and γ_{blue}, and the values of $\mathcal{E}(\boldsymbol{f},\hat{\boldsymbol{f}})$ and Δ_{SNR} are given in Table VII. The restored image $\hat{\boldsymbol{f}}$ by means of the constrained least squares filter for the degraded images $\boldsymbol{g}$ in Figs. 2(a) and 3(a) are given in Fig. 6. These results are too blurred and it is shown that the results by our proposed hyperparameter determination method constructed by means of the maximization of evidence are better than those by the familiar filter theory. Though the constrained least mean square filter can be regarded as a linear filter, we have a median filter and a mode filter as familiar nonlinear filters in signal processing. A vector median filter [24], a generalized vector directional filter [25] and an edge-preserved mode filter [26] were proposed as an extension of the median filter and the mode filter for vector-valued signals, respectively. In a generalized vector directional filter [25], we introduce a quantity $\theta_{x,y}$ as

TABLE IV. Values of $\hat{\sigma}$, $\hat{\nu}$, $\hat{\boldsymbol{\alpha}}$, $\mathcal{E}(\boldsymbol{f},\hat{\boldsymbol{f}})$ and Δ_{SNR} (dB) for the proposed model.

σ^*	$\hat{\sigma}$	$\hat{\boldsymbol{\alpha}}=\begin{pmatrix} \hat{\alpha}_{\mathrm{red,red}} & \hat{\alpha}_{\mathrm{red,green}} & \hat{\alpha}_{\mathrm{red,blue}} \\ \hat{\alpha}_{\mathrm{green,red}} & \hat{\alpha}_{\mathrm{green,green}} & \hat{\alpha}_{\mathrm{green,blue}} \\ \hat{\alpha}_{\mathrm{blue,red}} & \hat{\alpha}_{\mathrm{blue,green}} & \hat{\alpha}_{\mathrm{blue,blue}} \end{pmatrix}$	$\hat{\nu}$	$\mathcal{E}(\boldsymbol{f},\hat{\boldsymbol{f}})$	Δ_{SNR}(dB)
		(a) Home			
30	28.728	$\begin{pmatrix} 0.02322 & -0.01705 & 0.00039 \\ -0.01705 & 0.03678 & -0.02410 \\ 0.00039 & -0.02410 & 0.02928 \end{pmatrix}$	1.40511	155.80	7.27648
40	37.570	$\begin{pmatrix} 0.01951 & -0.01495 & 0.00090 \\ -0.01495 & 0.03452 & -0.02318 \\ 0.00090 & -0.02318 & 0.02752 \end{pmatrix}$	1.35600	204.51	8.45540
50	45.836	$\begin{pmatrix} 0.01694 & -0.01347 & 0.00117 \\ -0.01347 & 0.03265 & -0.02203 \\ 0.00117 & -0.02203 & 0.02575 \end{pmatrix}$	1.31700	253.62	9.26676
		(b) Mandrill			
30	29.299	$\begin{pmatrix} 0.00697 & -0.00830 & 0.00390 \\ -0.00830 & 0.01755 & -0.01138 \\ 0.00390 & -0.01138 & 0.00961 \end{pmatrix}$	1.01800	304.91	4.34334
40	38.133	$\begin{pmatrix} 0.00634 & -0.00759 & 0.00376 \\ -0.00759 & 0.01692 & -0.01136 \\ 0.00376 & -0.01136 & 0.00982 \end{pmatrix}$	1.01700	416.86	5.35158
50	46.494	$\begin{pmatrix} 0.00622 & -0.00752 & 0.00393 \\ -0.00752 & 0.01743 & -0.01197 \\ 0.00393 & -0.01197 & 0.01049 \end{pmatrix}$	1.02400	519.96	6.14037

$$\theta_{x,y}=\sum_{(x',y')\in \mathbf{w}_{x,y}} \mathcal{A}(\vec{g}_{x,y},\vec{g}_{x',y'}), \tag{3.19}$$

where $\mathcal{A}(\vec{g}_{x,y},\vec{g}_{x',y'})$ denotes the angle between the vectors $\vec{g}_{x,y}$ and $\vec{g}_{x',y'}$, $0\leqq\mathcal{A}(\vec{g}_{x,y},\vec{g}_{x',y'})\leqq\pi$ and $\mathbf{w}_{x,y}\equiv\{(x',y')|x'=x-1,x,x+1,\ y'=y-1,y,y+1\}$. We define an ordering of elements in the set $\{\vec{g}_{x',y'}|(x',y')\in\mathbf{w}_{x,y}\}$ as follows:

$$\vec{g}^{(1)}_{x,y}\leqq\vec{g}^{(2)}_{x,y}\leqq\cdots\leqq\vec{g}^{(k)}_{x,y}\leqq\cdots\leqq\vec{g}^{(9)}_{x,y}, \tag{3.20}$$

according to the ordering of elements in the set $\{\theta_{x',y'}|(x',y')\in\mathbf{w}_{x,y}\}$,

$$\theta^{(1)}_{x,y}\leqq\theta^{(2)}_{x,y}\leqq\cdots\leqq\theta^{(k)}_{x,y}\leqq\cdots\leqq\theta^{(9)}_{x,y}. \tag{3.21}$$

The first k terms of the ordering sequence, $\{\vec{g}^{(1)}_{x',y'},\vec{g}^{(2)}_{x',y'},\ldots,\vec{g}^{(k)}_{x',y'}\}$, constitute the output of the generalized vector directional filter. We define the set of the first k terms of the ordering sequence $\{\vec{g}^{(i)}_{x,y}|i=1,2,\ldots,k\}$. From the first $k=7$ terms of the ordering sequence for each window $\mathbf{w}_{x,y}$, the color $(\hat{f}_{x,y,\mathrm{red}},\hat{f}_{x,y,\mathrm{green}},\hat{f}_{x,y,\mathrm{blue}})$ for the restored image $\hat{\boldsymbol{f}}$ is determined by means of an α-trimmed

TABLE V. Values of $\hat{\sigma}$, $\hat{\boldsymbol{\alpha}}$, $\mathcal{E}(\boldsymbol{f},\hat{\boldsymbol{f}})$ and Δ_{SNR} (dB) for the multichannel CAR model ($\nu=1$).

σ^*	$\hat{\sigma}$	$\hat{\boldsymbol{\alpha}}=\begin{pmatrix} \hat{\alpha}_{\mathrm{red,red}} & \hat{\alpha}_{\mathrm{red,green}} & \hat{\alpha}_{\mathrm{red,blue}} \\ \hat{\alpha}_{\mathrm{green,red}} & \hat{\alpha}_{\mathrm{green,green}} & \hat{\alpha}_{\mathrm{green,blue}} \\ \hat{\alpha}_{\mathrm{blue,red}} & \hat{\alpha}_{\mathrm{blue,green}} & \hat{\alpha}_{\mathrm{blue,blue}} \end{pmatrix}$	$\mathcal{E}(\boldsymbol{f},\hat{\boldsymbol{f}})$	Δ_{SNR}(dB)
		(a) Home		
30	26.670	$\begin{pmatrix} 0.00594 & -0.00293 & -0.00081 \\ -0.00293 & 0.00709 & -0.00393 \\ -0.00081 & -0.00393 & 0.00654 \end{pmatrix}$	176.82	6.72690
40	35.713	$\begin{pmatrix} 0.00514 & -0.00269 & -0.00057 \\ -0.00269 & 0.00708 & -0.00420 \\ -0.00057 & -0.00420 & 0.00654 \end{pmatrix}$	227.12	7.99997
50	44.144	$\begin{pmatrix} 0.00466 & -0.00260 & -0.00039 \\ -0.00260 & 0.00732 & -0.00450 \\ -0.00039 & -0.00450 & 0.00668 \end{pmatrix}$	276.16	8.89690
		(b) Mandrill		
30	29.172	$\begin{pmatrix} 0.00649 & -0.00753 & 0.00347 \\ -0.00753 & 0.01595 & -0.01030 \\ 0.00347 & -0.01030 & 0.00881 \end{pmatrix}$	304.37	4.35106
40	38.006	$\begin{pmatrix} 0.00590 & -0.00688 & 0.00335 \\ -0.00688 & 0.01536 & -0.01027 \\ 0.00335 & -0.01027 & 0.00899 \end{pmatrix}$	416.06	5.35991
50	46.307	$\begin{pmatrix} 0.00558 & -0.00651 & 0.00332 \\ -0.00651 & 0.01511 & -0.01033 \\ 0.00332 & -0.01033 & 0.00920 \end{pmatrix}$	518.86	6.14950

means filter ($\alpha=1/9$) after re-ordering the set $\{\vec{g}^{(i)}_{x,y}|\ i=1,2,\ldots,k\}$ for the magnitude. We give in Table VIII thevalues of $\mathcal{E}(\boldsymbol{f},\hat{\boldsymbol{f}})$ and Δ_{SNR} in the generalized vector directional filter for the degraded images $\boldsymbol{g}$ obtained from the original images $\boldsymbol{f}$ in Fig. 1 by setting $\sigma^*=30$, 40, and 50 in the degradation process (2.1). We give in Fig. 7 the restored image $\hat{\boldsymbol{f}}$ by means of the generalized vector directional filter for the degraded images $\boldsymbol{g}$ in Figs. 2(a) and 3(a). We also did some numerical experiments by means of a vector median filter [24] and obtained worse results than those by the generalized vector directional filter. In an edge-preserving filter [26], we calculate the restored image $\boldsymbol{z}'=\{\vec{z}'_{x,y}|(x,y)\in\mathbf{L}\}$ in the $L^*a^*b^*$ representation

$$\vec{z}'_{x,y}=\frac{\sum_{(x',y')\in\mathbf{L}}\vec{g}'_{x',y'}\exp\{-\alpha[(x-x')^2+(y-y')^2]-\beta||\vec{g}'_{x,y}-\vec{g}'_{x',y'}||\}}{\sum_{(x',y')\in\mathbf{L}}\exp\{-\alpha[(x-x')^2+(y-y')^2]-\beta||\vec{g}'_{x,y}-\vec{g}'_{x',y'}||\}}, \tag{3.22}$$

TABLE VI. Values of $\hat{\sigma}$, $\hat{\boldsymbol{\alpha}}$, $\mathcal{E}(\boldsymbol{f},\hat{\boldsymbol{f}})$ and Δ_{SNR} (dB) for the multichannel SAR model ($\nu=2$).

σ^*	$\hat{\sigma}$	$\hat{\boldsymbol{\alpha}}=\begin{pmatrix} \hat{\alpha}_{\mathrm{red,red}} & \hat{\alpha}_{\mathrm{red,green}} & \hat{\alpha}_{\mathrm{red,blue}} \\ \hat{\alpha}_{\mathrm{green,red}} & \hat{\alpha}_{\mathrm{green,green}} & \hat{\alpha}_{\mathrm{green,blue}} \\ \hat{\alpha}_{\mathrm{blue,red}} & \hat{\alpha}_{\mathrm{blue,green}} & \hat{\alpha}_{\mathrm{blue,blue}} \end{pmatrix}$	$\mathcal{E}(\boldsymbol{f},\hat{\boldsymbol{f}})$	Δ_{SNR}(dB)
		(a) Home		
30	30.000	$\begin{pmatrix} 0.20098 & -0.20533 & 0.05679 \\ -0.20533 & 0.44136 & -0.31119 \\ 0.05679 & -0.31119 & 0.30589 \end{pmatrix}$	162.40	7.09628
40	39.030	$\begin{pmatrix} 0.26091 & -0.28542 & 0.09199 \\ -0.28542 & 0.64120 & -0.45685 \\ 0.09199 & -0.45685 & 0.43440 \end{pmatrix}$	214.53	8.24766
50	47.416	$\begin{pmatrix} 0.33004 & -0.37709 & 0.13047 \\ -0.37709 & 0.85882 & -0.60620 \\ 0.13047 & -0.60620 & 0.56033 \end{pmatrix}$	267.42	9.03658
		(b) Mandrill		
30	33.093	$\begin{pmatrix} 0.53472 & -1.09612 & 0.73344 \\ -1.09612 & 2.42766 & -1.68841 \\ 0.73344 & -1.68841 & 1.19876 \end{pmatrix}$	379.64	3.39126
40	42.761	$\begin{pmatrix} 0.69536 & -1.47065 & 1.00241 \\ -1.47065 & 3.38804 & -2.39807 \\ 1.00241 & -2.39807 & 1.73028 \end{pmatrix}$	544.34	4.19273
50	51.327	$\begin{pmatrix} 0.78080 & -1.68688 & 1.14999 \\ -1.68688 & 4.03726 & -2.86030 \\ 1.14999 & -2.86031 & 2.06781 \end{pmatrix}$	683.62	4.95187

after replacing the degraded image $\boldsymbol{g}$ in the RGB representation by the image $\boldsymbol{g}'=\{\vec{g}'_{x,y}|(x,y)\in\mathbf{L}\}$ in the $L^*a^*b^*$ representation [10]. The restored image $\hat{\boldsymbol{f}}$ is obtained from the image $\boldsymbol{z}'$ by using the inverse transformation from the $L^*a^*b^*$ representation to the RGB representation. We give the values of $\mathcal{E}(\boldsymbol{f},\hat{\boldsymbol{f}})$ and Δ_{SNR} in the edge-preserved mode filter in Table IX for the degraded images $\boldsymbol{g}$ obtained from the original images $\boldsymbol{f}$ in Fig. 1 by setting $\sigma^*=30$, 40, and 50 in the degradation process (2.1). The restored images $\hat{\boldsymbol{f}}$ by means of the edge-preserved mode filter for the degraded images $\boldsymbol{g}$ in Figs. 2(a) and 3(a) are given in Fig. 8. In the nonlinear filters, the edges tend to be preserved and are not too blurred; some noises also remain. It is shown that the results by our proposed hyperparameter determination method constructed by means of the maximization of evidence are better than those by the familiar linear filter theory and also by the familiar nonlinear filter theory.

IV. CONCLUDING REMARKS

In this paper, we have proposed a solvable MRF model for image restoration of full color images. The framework of the hyperparameter determination has been formulated by means of the maximization of evidence. The exact expression of the evidence and the restored image for a given degraded image have been obtained. The deterministic equations for hyperparameters have been derived exactly. The proposed model includes both the multichannel CAR model and the multichannel SAR model for color image restoration as a special case. Some noise could not be erased by the multichannel CAR model, while the most of all noises have been suppressed by the multichannel SAR model. On the other hand, the contours of the image remain by the multichannel CAR model, though the restored image has been blurred by the multi-channel SAR model. However, the proposed probabilistic model gives good results for the image

restoration of full color images. In the restored image, the major contours are conserved and the most of all noises are erased.

All hyperparameters in our proposed probabilistic model are determined automatically only from a given degraded image. Particularly, the hyperparameter

$$\boldsymbol{\alpha}=\begin{pmatrix} \alpha_{\mathrm{red,red}} & \alpha_{\mathrm{red,green}} & \alpha_{\mathrm{red,blue}} \\ \alpha_{\mathrm{green,red}} & \alpha_{\mathrm{green,green}} & \alpha_{\mathrm{green,blue}} \\ \alpha_{\mathrm{blue,red}} & \alpha_{\mathrm{blue,green}} & \alpha_{\mathrm{blue,blue}} \end{pmatrix}$$

expresses a correlation between different colors. One of important points of color image processing is how we treat a correlation and an interaction between different color planes. Actually, the results obtained in our numerical experiments show that the amplitude of interactions between different color planes has the similar order as the ones in the same color planes.

In our numerical experiments, we have given a comparison between the present method and some linear and nonlinear filters [23–26]. We have shown that the results by our proposed hyperparameter determination method constructed by means of the maximization of evidence are better than those by the familiar filters. In the constrained least squares filter given in Eq. (3.15), it is difficult to treat correlations between different planes in the RGB space, though we believe that color images should have correlations between different planes in the RGB space. Our proposed method in the present paper can easily treat such correlations between different planes in the RGB space, as a 3×3 matrix $\boldsymbol{\alpha}$. It is interesting to compare the results by our proposed method with the constrained least squares filter constructed in the other color representation where the different planes have no correlation with each other. Angelopoulos and Pitas [6] dealt with a design of multichannel Wiener filter in the RGB space, based on a multichannel autoregressive model and familiar signal processing techniques. Their formulation included correlations between different planes in the RGB space. However, their main purpose is to design an optimal filter that gives us the least-square estimate of the original image $\boldsymbol{f}$ and their method is based on the minimization of a statistical average in the mean square error between the original image $\boldsymbol{f}$ and the degraded image $\boldsymbol{g}$. In designing their optimal filter, they have to estimate a statistical correlation between the original image $\boldsymbol{f}$ and the degraded image $\boldsymbol{g}$. They have used the original image $\boldsymbol{f}$ to determine the coefficients in their filter, which correspond to the hyperparameters in our proposed model. Moreover, we have compared the results by our proposed method with those by some nonlinear filters that are referred as the generalized vector directional filter [25] and the edge-preserved mode filter [26]. In the nonlinear filters, some noises still remain in the restored images and the mean square error is not so good though the edges are preserved.

Kato *et al.* [8] and Kang and Roh [9] constructed a probabilistic model not in the RGB space but in the $L^*u^*v^*$ space for color image segmentation. It is known that the $L^*u^*v^*$ color space and the $L^*a^*b^*$ color space are similar to human color perception capability [10]. In the Bayesian approach of a probabilistic model for color image restoration, the degradation process and the *a priori* probability distribution should be assumed in the same color space as each other. If these probabilistic distributions are given in the different color space of each others, the corresponding energy function in the *a posteriori* probability distribution has very complicated structure and it is difficult to treat it analytically. It is easy to construct a solvable probabilistic model, which is corresponding to the proposed model, in the $L^*u^*v^*$ color space or in the $L^*a^*b^*$ color space if the degradation process is given as an additive white Gaussian noise in the $L^*u^*v^*$ color space or in the $L^*a^*b^*$ color space.

Moreover, a scheme proposed by Kang and Roh [9] increases the performance of segmentation by introducing not only a smoothing factor but also an edge-preserving factor in the energy function. Also in the present model, the performance of color image restoration can be increased by introducing an edge-preserving factor, for example, line fields. Jeng and Woods [21,22] proposed a compound Gauss-Markov random field model which is constructed by introducing line fields as Markov random fields to Gaussian model for gray-level monochrome image restoration and showed that the model gives us high performance in image restoration. However, it is difficult to treat such probabilistic

TABLE VII. Values of γ_{red}, γ_{green}, γ_{blue}, $\mathcal{E}(\boldsymbol{f},\hat{\boldsymbol{f}})$ and Δ_{SNR} (dB) in image restorations by using the constrained least squares filter.

σ^*	γ_{red}	γ_{green}	γ_{blue}	$\mathcal{E}(\boldsymbol{f},\hat{\boldsymbol{f}})$	Δ_{SNR} (dB)
			(a) Home		
30	35.035	23.593	41.527	242.99	5.34639
40	100.175	77.449	228.707	342.24	6.21913
50	510.726	502.799	2984.813	521.14	6.13898
			(b) Mandrill		
30	7.718	4.424	4.859	506.70	2.13748
40	24.024	10.641	13.788	642.96	3.46964
50	134.322	31.970	59.829	767.42	4.44971

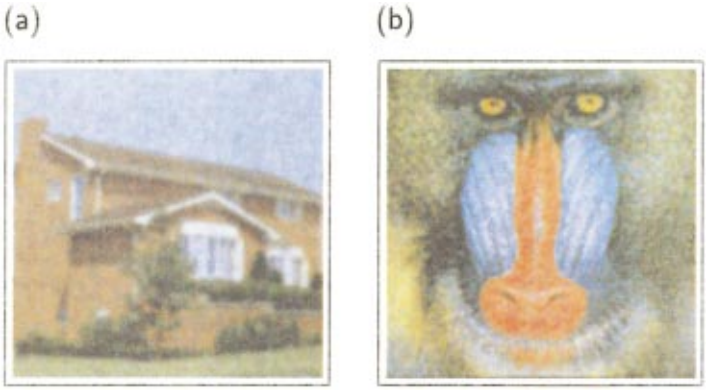

FIG. 6. (Color) Image restorations by using the constrained least squares filter. (a) Restored image $\hat{\boldsymbol{f}}$ for the degraded image $\boldsymbol{g}$ in Fig. 2(a). (b) Restored image $\hat{\boldsymbol{f}}$ for the degraded image $\boldsymbol{g}$ in Fig. 3(a).

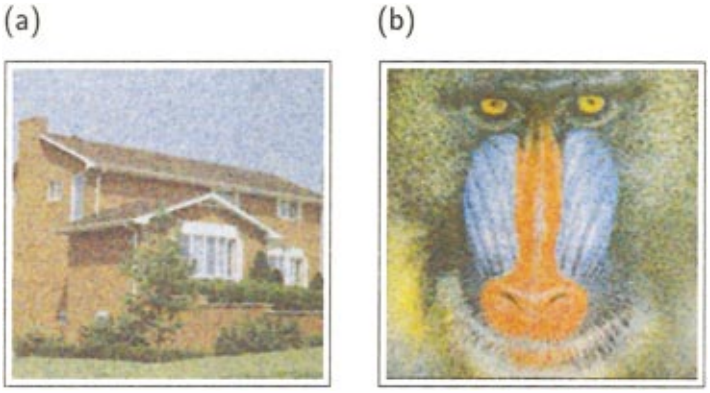

FIG. 7. (Color) Image restorations by using the generalized vector directional filter ($k=7$, $\alpha=1/9$). (a) Restored image $\hat{\boldsymbol{f}}$ for the degraded image $\boldsymbol{g}$ in Fig. 2(a). (b) Restored image $\hat{\boldsymbol{f}}$ for the degraded image $\boldsymbol{g}$ in Fig. 3(a).

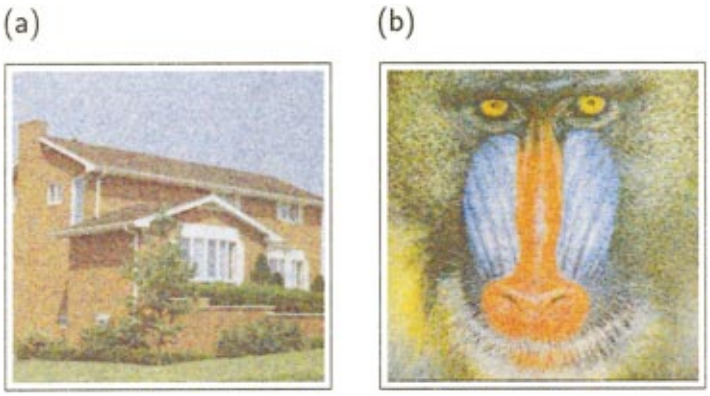

FIG. 8. (Color) Image restorations by using the edge-preserved mode filter ($\alpha=2.0$, $\beta=0.000\,005\,0$). (a) Restored image $\hat{\boldsymbol{f}}$ for the degraded image $\boldsymbol{g}$ in Fig. 2(a). (b) Restored image $\hat{\boldsymbol{f}}$ for the degraded image $\boldsymbol{g}$ in Fig. 3(a).

models with line fields or segmentation fields exactly and we have to employ a statistical-mechanical approximation. This is left as a future problem.

In the present paper, we have assumed the additive white Gaussian model as a degradation process. The additive white Gaussian noise is the most popular noise. Generally, the degradation process treated in image processing is given by

$$g_{x,y,\kappa}-\sum_{(x',y')\in\mathbf{L}}\sum_{\kappa'\in\mathbf{K}}\langle\kappa|\boldsymbol{B}(|x-x'|,|y-y'|)|\kappa'\rangle f_{x',y',\kappa'} \sim\mathcal{N}[0,\sigma^2] \quad [(x,y)\in\mathbf{L},\ \kappa\in\mathbf{K}]. \tag{4.1}$$

Here, $\boldsymbol{B}(|x-x'|,|y-y'|)$ is a 3×3 matrix and denotes ablurring noise. On the other hand, $\mathcal{N}[0,\sigma^2]$ is an additive

TABLE VIII. Values of $\mathcal{E}(\boldsymbol{f},\hat{\boldsymbol{f}})$ and Δ_{SNR} (dB) in image restorations by using the generalized vector directional filter ($k=7$, $\alpha=1/9$).

σ*	$\mathcal{E}(\boldsymbol{f},\hat{\boldsymbol{f}})$	Δ_{SNR} (dB)
	(a) Home	
30	422.01	2.94893
40	572.86	3.98198
50	756.19	4.52225
	(b) Mandrill	
30	953.80	−0.60954
40	1095.81	1.15413
50	1264.30	2.28152

TABLE IX. Values of $\mathcal{E}(\boldsymbol{f},\hat{\boldsymbol{f}})$ and Δ_{SNR} (dB) in image restorations by using the edge-preserved mode filter ($\alpha=2.0$, $\beta=0.000\,005\,0$).

σ*	$\mathcal{E}(\boldsymbol{f},\hat{\boldsymbol{f}})$	Δ_{SNR} (dB)
	(a) Home	
30	293.26	4.52964
40	492.25	4.64058
50	740.90	4.61095
	(b) Mandrill	
30	435.35	2.79668
40	636.10	3.51619
50	883.57	3.83760

TABLE X. Values of $\mathcal{V}_{\kappa,\kappa''}[\boldsymbol{f}]$ ($\kappa,\kappa''=$red, green, blue).

	$\kappa''=$red	$\kappa''=$green	$\kappa''=$blue
	(a) Home		
$\kappa=$red	100.97	1525.52	2643.45
$\kappa=$green	1614.90	150.75	919.53
$\kappa=$blue	2697.07	883.76	133.72
	(b) Mandrill		
$\kappa=$red	546.98	3807.21	6099.80
$\kappa=$green	3984.93	790.69	1853.35
$\kappa=$blue	6283.69	1859.52	794.86

white Gaussian noise. The case treated in the present paper corresponds to the one in setting $\langle\kappa|\boldsymbol{B}(x,y)|\kappa'\rangle=\delta_{x,0}\delta_{y,0}\delta_{\kappa,\kappa'}$. It is believed that the additive white Gaussian noise given in Eq. (2.1) is realistic in the case that a degraded image $\boldsymbol{g}$ is produced from an original image by changing the grade of each pixel to another grade by a probability independently of the other pixels. For a more realistic application, we have to treat the degradation process (4.1). In this general case, we have to estimate also the matrix $\boldsymbol{B}(x,y)$ as hyperparameters. This is also left as a future problem.

Finally, we explain a motivation of our *a priori* probability density function in Eqs. (2.4), (2.5), and (2.7) and mention a generalization of our proposed model. In the proposed model in the present paper, the expression of the evidence can be calculated analytically and the iterated algorithm to determine the hyperparameters can be given easily. As one of more general cases, we can consider the following *a priori* probability density function:

$$\rho\{\boldsymbol{F}=\boldsymbol{f}|\{\mathcal{R}_{\kappa,\kappa'}^{\kappa'',\kappa'''}\},\nu\}\equiv\frac{\exp\left(-\frac{1}{2}\sum_{\kappa\in\mathbf{K}}\sum_{\kappa'\in\mathbf{K}}\sum_{\kappa''\in\mathbf{K}}\sum_{\kappa'''\in\mathbf{K}}\mathcal{R}_{\kappa,\kappa'}^{\kappa'',\kappa'''}\boldsymbol{f}^{T}\boldsymbol{A}(\kappa,\kappa',\kappa'',\kappa''')^{\nu}\boldsymbol{f}\right)}{\int\exp\left(-\frac{1}{2}\sum_{\kappa\in\mathbf{K}}\sum_{\kappa'\in\mathbf{K}}\sum_{\kappa''\in\mathbf{K}}\sum_{\kappa'''\in\mathbf{K}}\mathcal{R}_{\kappa,\kappa'}^{\kappa'',\kappa'''}\boldsymbol{z}^{T}\boldsymbol{A}(\kappa,\kappa',\kappa'',\kappa''')^{\nu}\boldsymbol{z}\right)d\boldsymbol{z}},\tag{4.2}$$

instead of Eqs. (2.4), (2.5), and (2.7). Here, $\boldsymbol{A}(\kappa,\kappa',\kappa'',\kappa''')$ $(\kappa,\kappa',\kappa'',\kappa'''\in\mathbf{K})$ is a $3|\mathbf{L}|\times3|\mathbf{L}|$ matrix whose $(x,y,\mu|x',y',\mu')$ element is defined by

$$\begin{aligned}&\langle x,y,\mu|\boldsymbol{A}(\kappa,\kappa',\kappa'',\kappa''')|x',y',\mu'\rangle\\&\quad\equiv\delta_{x,x'}\delta_{y,y'}\delta_{\kappa,\mu}\delta_{\kappa',\mu'}-\frac{1}{4}\delta_{\kappa'',\mu}\delta_{\kappa''',\mu'}\\&\qquad\times(\delta_{x,x'+1}\delta_{y,y'}+\delta_{x,x'-1}\delta_{y,y'}\\&\qquad+\delta_{x,x'}\delta_{y,y'+1}+\delta_{x,x'}\delta_{y,y'-1})\\&\qquad[(x,y),(x',y')\in\mathbf{L},\quad\mu,\mu'\in\mathbf{K}].\end{aligned}\tag{4.3}$$

The energy function for $\nu=2$ is rewritten as follows:

$$\begin{aligned}&\frac{1}{2}\sum_{\kappa\in\mathbf{K}}\sum_{\kappa'\in\mathbf{K}}\sum_{\kappa''\in\mathbf{K}}\sum_{\kappa'''\in\mathbf{K}}\mathcal{R}_{\kappa,\kappa'}^{\kappa'',\kappa'''}\boldsymbol{f}^{\mathrm{T}}\boldsymbol{A}(\kappa,\kappa',\kappa'',\kappa''')^{2}\boldsymbol{f}\\&\quad=\sum_{(x,y)\in\mathbf{L}}\sum_{\kappa\in\mathbf{K}}\sum_{\kappa'\in\mathbf{K}}\sum_{\kappa''\in\mathbf{K}}\sum_{\kappa'''\in\mathbf{K}}\mathcal{R}_{\kappa,\kappa'}^{\kappa'',\kappa'''}\\&\qquad\times\left(f_{x,y,\kappa}-\frac{1}{4}(f_{x+1,y,\kappa''}+f_{x-1,y,\kappa''}+f_{x,y+1,\kappa''}\right.\\&\qquad\left.+f_{x,y-1,\kappa''})\right)\left(f_{x,y,\kappa'}-\frac{1}{4}(f_{x+1,y,\kappa'''}+f_{x-1,y,\kappa'''}\right.\\&\qquad\left.+f_{x,y+1,\kappa'''}+f_{x,y-1,\kappa'''})\right).\end{aligned}\tag{4.4}$$

In the original images $\boldsymbol{f}$ given in Fig. 1, the values $\mathcal{V}_{\kappa,\kappa''}[\boldsymbol{f}]$ $(\kappa,\kappa''\in\mathbf{K})$ are given in Table X, where $\mathcal{V}_{\kappa,\kappa''}[\boldsymbol{f}]$ are defined

by

$$\mathcal{V}_{\kappa,\kappa''}[\boldsymbol{f}] \equiv \sum_{(x,y)\in\mathbf{L}} \left[\left(f_{x,y,\kappa} - \frac{1}{4}(f_{x+1,y,\kappa''} + f_{x-1,y,\kappa''} + f_{x,y+1,\kappa''} + f_{x,y-1,\kappa''}) \right) - \mathcal{E}_{\kappa,\kappa''}[\boldsymbol{f}] \right]^2, \tag{4.5}$$

$$\mathcal{E}_{\kappa,\kappa''}[\boldsymbol{f}] \equiv \sum_{(x,y)\in\mathbf{L}} \left(f_{x,y,\kappa} - \frac{1}{4}(f_{x+1,y,\kappa''} + f_{x-1,y,\kappa''} + f_{x,y+1,\kappa''} + f_{x,y-1,\kappa''}) \right). \tag{4.6}$$

Since we see that the variance $\mathcal{V}_{\kappa,\kappa''}[\boldsymbol{f}]$ $(\kappa \neq \kappa'',\ \kappa,\kappa'' \in \mathbf{K})$ is much larger than $\mathcal{V}_{\kappa,\kappa}[\boldsymbol{f}]$ $(\kappa \in \mathbf{K})$, we can regard the coefficients $\mathcal{R}_{\kappa,\kappa'}^{\kappa'',\kappa'''}$ for the case of $\kappa \neq \kappa''$ or of $\kappa' \neq \kappa'''$ to be much smaller than $\mathcal{R}_{\kappa,\kappa'}^{\kappa,\kappa'}$ in the *a priori* probability density function $\rho\{\boldsymbol{F}=\boldsymbol{f}|\{\mathcal{R}_{\kappa,\kappa'}^{\kappa'',\kappa'''}\},\nu\}$ for the original image $\boldsymbol{f}$. If we consider not only the coefficients $\mathcal{R}_{\kappa,\kappa'}^{\kappa,\kappa'}$ but also $\mathcal{R}_{\kappa,\kappa'}^{\kappa'',\kappa'''}$, the number of hyperparameters in the *a priori* probability density function is 81 and it is much hard to calculate the optimal point in the set of hyperparameters by means of the evidence framework. In order to treat the most basic case, we set $\mathcal{R}_{\kappa,\kappa'}^{\kappa'',\kappa'''} = \delta_{\kappa,\kappa''}\delta_{\kappa',\kappa'''}\alpha_{\kappa,\kappa'}$ in the present paper, as shown in Eqs. (2.4), (2.5), and (2.7). The matrix $\boldsymbol{A}(\kappa,\kappa',\kappa'',\kappa''')$ has translational symmetry and then can be diagonalized by means of the unitary matrix $\boldsymbol{U}$ in Eq. (2.16) as follows:

$$\begin{aligned}\langle p,q,\mu|\boldsymbol{U}^{-1}\boldsymbol{A}(\kappa,\kappa',\kappa'',\kappa''')\boldsymbol{U}|p',q',\mu'\rangle \\ = \delta_{p,p'}\delta_{q,q'} \times \left\{ \delta_{\kappa,\mu}\delta_{\kappa',\mu'} - \frac{1}{2}\delta_{\kappa'',\mu}\delta_{\kappa''',\mu'} \right. \\ \left. \times \left[\cos\left(\frac{2\pi p}{L_x}\right) + \cos\left(\frac{2\pi q}{L_y}\right) \right] \right\}.\end{aligned} \tag{4.7}$$

Hence, it is also possible to treat the above generalized probabilistic model by means of the evidence framework, analytically, in the similar way to the present paper. It is a future problem to investigate the efficiency of the extended probabilistic color image processing with the *a priori* probability density function given in Eqs. (4.2) and (4.3).

[1] H. Nishimori, *Statistical Physics of Spin Glasses and Information Processing, An Introduction* (Oxford University Press, Cambridge, 2001).

[2] H. Derin, H. Elliott, R. Cristi, and D. Geman, IEEE Trans. Pattern Anal. Mach. Intell. **6**, 707 (1984).

[3] S. Geman and D. Geman, IEEE Trans. Pattern Anal. Mach. Intell. **6**, 721 (1984).

[4] *Markov Random Fields*: *Theory and Applications*, edited by R. Chellappa and A. Jain (Academic Press, New York, 1993).

[5] S.Z. Li, *Markov Random Field Modeling in Computer Vision* (Springer-Verlag, Tokyo, 1995).

[6] G. Angelopoulos and I. Pitas, IEEE Trans. Circuits Syst. Video Technol. **4**, 83 (1994).

[7] D.K. Panjwani and G. Healey, IEEE Trans. Pattern Anal. Mach. Intell. **17**, 939 (1995).

[8] Z. Kato, T.C. Pong, and J.C.M. Lee, Pattern Recogn. Lett. **22**, 309 (2001).

[9] D.J. Kang and K.S. Roh, Image Vis. Comput. **19**, 369 (2001).

[10] G. Wyszecki and W.S. Stiles, *Color Science: Concepts and Methods, Quantitative Data and Formula* (Wiley, New York, 1982).

[11] R. Vicente, D. Saad, and Y. Kabashima, Europhys. Lett. **51**, 698 (2000).

[12] H. Nishimori and K.Y.M. Wong, Phys. Rev. E **60**, 132 (1999).

[13] H. Nishimori, BUSSEI KENKYU **73**, 850 (2000) (in Japanese).

[14] R. Molina, IEEE Trans. Pattern Anal. Mach. Intell. **16**, 1122 (1994).

[15] K. Tanaka and J. Inoue, IEICE Trans., **E-85D**, 546 (2002).

[16] D.J. MacKay, Neural Comput. **4**, 415 (1992).

[17] J.M. Pryce and A.D. Bruce, J. Phys. A **28**, 511 (1995).

[18] Z. Zhou, R.M. Leahy, and J. Qi, IEEE Trans. Image Process. **6**, 844 (1997).

[19] J. Marroquin, S. Mitter, and T. Poggio, J. Am. Stat. Assoc. **82**, 76 (1987).

[20] H. Nishimori, J. Phys. Soc. Jpn. **62**, 2973 (1993).

[21] F.C. Jeng and J.W. Woods, IEEE Trans. Inf. Theory **36**, 94 (1990).

[22] F.C. Jeng and J.W. Woods, IEEE Trans. Signal Process. **39**, 683 (1991).

[23] B.R. Hunt, IEEE Trans. Comput. **22**, 805 (1973).

[24] J. Astola, P. Haavisto, and Y. Neuvo, Proc. IEEE **78**, 678 (1990).

[25] P.E. Trahanias and A.N. Venetsanopoulos, IEEE Trans. Image Process. **2**, 528 (1993).

[26] M. Okada and K. Urahama, IEICE Trans. **J81-A**, 1189 (1998).